(MEXT) and the 3rd Term Comprehensive Control Research for Cancer from the Ministry of Health, Labor and Welfare of Japan (MHLW).

Conflict of Interest
None declared.

References

1. Kageyama, S., Isono, T., Iwaki, H., Wakabayashi, Y., Okada, Y., Kontani, K., Yoshimura, K., Terai, A., Arai, Y., and Yoshiki, T. (2004) Identification by proteomic analysis of calreticulin as a marker for bladder cancer and evaluation of the diagnostic accuracy of its detection in urine. *Clin. Chem.* **50**, 857–866
2. Kageyama, S., Iwaki, H., Inoue, H., Isono, T., Yuasa, T., Nogawa, M., Maekawa, T., Ueda, M., Kajita, Y., Ogawa, O., Toguchida, J., and Yoshiki, T. (2007) A novel tumor-related protein, C7orf24, identified by proteome differential display of bladder urothelial carcinoma. *Proteomics Clin. Appl.* **1**, 192–199
3. Zhang, C., Li, H.R., Fan, J.B., Wang-Rodriguez, J., Downs, T., Fu, X.D., and Zhang, M.Q. (2006) Profiling alternatively spliced mRNA isoforms for prostate cancer classification. *BMC Bioinformatics* **7**, 202
4. Xu, L., Geman, D., and Winslow, R.L. (2007) Large-scale integration of cancer microarray data identifies a robust common cancer signature. *BMC Bioinformatics* **8**, 275
5. Gromov, P., Gromova, I., Friis, E., Timmermans-Wielenga, V., Rank, F., Simon, R., Sauter, G., and Moreira, J.M. (2010) Proteomic profiling of mammary carcinomas identifies C7orf24, a gamma-glutamyl cyclotransferase, as a potential cancer biomarker. *J. Proteome Res.* **9**, 3941–3953
6. Uejima, D., Nishijo, K., Kajita, Y., Ishibe, T., Aoyama, T., Kageyama, S., Iwaki, H., Nakamura, T., Iida, H., Yoshiki, T., and Toguchida, J. (2011) Involvement of cancer biomarker C7orf24 in the growth of human osteosarcoma. *Anticancer Res.* **31**, 1297–1305
7. Azumi, K., Ikeda, Y., Takeuchi, T., Nomura, T., Sabau, S.V., Hamada, J., Okada, F., Hosokawa, M., and Yokosawa, H. (2009) Localization and characterization of gamma-glutamyl cyclotransferase in cancer cells. *Mol. Med. Rep.* **2**, 385–391
8. Oakley, A.J., Yamada, T., Liu, D., Coggan, M., Clark, A.G., and Board, P.G. (2008) The identification and structural characterization of C7orf24 as gamma-glutamyl cyclotransferase. An essential enzyme in the gamma-glutamyl cycle. *J. Biol. Chem.* **283**, 22031–22042
9. Oakley, A.J., Coggan, M., and Board, P.G. (2010) Identification and characterization of gamma-glutamylamine cyclotransferase, an enzyme responsible for gamma-glutamyl-epsilon-lysine catabolism. *J. Biol. Chem.* **285**, 9642–9648
10. Ohno, Y., Hattori, A., Ueda, M., Kageyama, S., Yoshiki, T., and Kakeya, H. (2011) Multiple NF-Y-binding CCAAT boxes are essential for transcriptional regulation of the human C7orf24 gene, a novel tumor-associated gene. *FEBS J.* **278**, 4088–4099
11. Sims, R.J., Nishioka, K., and Reinberg, D. (2003) Histone lysine methylation: a signature for chromatin function. *Trends Genet.* **19**, 629–639
12. Mellor, J. (2006) Dynamic nucleosomes and gene transcription. *Trends Genet.* **22**, 320–329
13. Margueron, R. and Reinberg, D. (2011) The Polycomb complex PRC2 and its mark in life. *Nature* **469**, 343–349
14. Esteller, M. (2008) Epigenetics in cancer. *N. Engl. J. Med.* **358**, 1148–1159
15. Klose, R.J. and Bird, A.P. (2006) Genomic DNA methylation: the mark and its mediators. *Trends Biochem. Sci.* **31**, 89–97
16. Sharma, S., Kelly, T.K., and Jones, P.A. (2010) Epigenetics in cancer. *Carcinogenesis* **31**, 27–36
17. Belinsky, S.A. (2004) Gene-promoter hypermethylation as a biomarker in lung cancer. *Nat. Rev. Cancer* **4**, 707–717
18. Liloglou, T., Bediaga, N.G., Brown, B.R., Field, J.K., and Davies, M.P. (2013) Epigenetic biomarkers in lung cancer. *Cancer Lett.*, in press
19. Jeronimo, C., Bastian, P.J., Bjartell, A., Carbone, G.M., Catto, J.W., Clark, S.J., Henrique, R., Nelson, W.G., and Shariat, S.F. (2011) Epigenetics in prostate cancer: biologic and clinical relevance. *Eur. Urol.* **60**, 753–766
20. Sakuma, M., Akahira, J., Ito, K., Niikura, H., Moriya, T., Okamura, K., Sasano, H., and Yaegashi, N. (2007) Promoter methylation status of the Cyclin D2 gene is associated with poor prognosis in human epithelial ovarian cancer. *Cancer Sci.* **98**, 380–386
21. Chernov, A.V., Sounni, N.E., Remacle, A.G., and Strongin, A.Y. (2009) Epigenetic control of the invasion-promoting MT1-MMP/MMP-2/TIMP-2 axis in cancer cells. *J. Biol. Chem.* **284**, 12727–12734
22. Wu, H., Chen, Y., Liang, J., Shi, B., Wu, G., Zhang, Y., Wang, D., Li, R., Yi, X., Zhang, H., Sun, L., and Shang, Y. (2005) Hypomethylation-linked activation of PAX2 mediates tamoxifen-stimulated endometrial carcinogenesis. *Nature* **438**, 981–987
23. Taniguchi, N. and Ikeda, Y. (1998) gamma-Glutamyl transpeptidase: catalytic mechanism and gene expression. *Adv. Enzymol. Relat. Areas Mol. Biol.* **72**, 239–278
24. Chikhi, N., Holic, N., Guellaen, G., and Laperche, Y. (1999) Gamma-glutamyl transpeptidase gene organization and expression: a comparative analysis in rat, mouse, pig and human species. *Comp. Biochem. Physiol. B Biochem. Mol. Biol.* **122**, 367–380
25. Yao, D., Jiang, D., Huang, Z., Lu, J., Tao, Q., Yu, Z., and Meng, X. (2000) Abnormal expression of hepatoma specific gamma-glutamyl transferase and alteration of gamma-glutamyl transferase gene methylation status in patients with hepatocellular carcinoma. *Cancer* **88**, 761–769
26. Baik, J.H., Siegrist, S., Giuili, G., Lahuna, O., Bulle, F., and Guellaen, G. (1992) Tissue- and developmental-stage-specific methylation in the two kidney promoters of the rat gamma-glutamyl transpeptidase gene. *Biochem. J.* **287 (Pt 3)**, 691–694
27. Coloma, J. and Garcia-Jimeno, A. (1991) Tissue-specific methylation in the 5' flanking region of the gamma-glutamyl transpeptidase gene. *Biochem. Biophys. Res. Commun.* **177**, 229–234
28. Fossati, A., Dolfini, D., Donati, G., and Mantovani, R. (2011) NF-Y recruits Ash2L to impart H3K4 trimethylation on CCAAT promoters. *PLoS One* **6**, e17220
29. Donati, G., Gatta, R., Dolfini, D., Fossati, A., Ceribelli, M., and Mantovani, R. (2008) An NF-Y-dependent switch of positive and negative histone methyl marks on CCAAT promoters. *PLoS One* **3**, e2066
30. Amano, T., Eishi, Y., Yamada, T., Uchida, K., Minegishi, K., Tamura, T., Kobayashi, D., Hiroshi, K., Suzuki, T., and Board, P.G. (2012) Widespread expression of gamma-glutamyl cyclotransferase suggests it is not a general tumor marker. *J. Histochem. Cytochem.* **60**, 76–86

Biochemical and Biophysical Research Communications 443 (2014) 950–956

Contents lists available at ScienceDirect

Biochemical and Biophysical Research Communications

journal homepage: www.elsevier.com/locate/ybbrc

Neovessel formation promotes liver fibrosis via providing latent transforming growth factor-β

Kotaro Sakata [a,b,c], Satoshi Eda [a], Eun-Seo Lee [a], Mitsuko Hara [a], Masaya Imoto [b], Soichi Kojima [a,*]

[a] Micro-signaling Regulation Technology Unit, RIKEN Center for Life Science Technologies, Wako, Saitama 351-0198, Japan
[b] Department of Biosciences and Informatics, Faculty of Science and Technology, Keio University, Yokohama, Kanagawa 223-8522, Japan
[c] Drug Discovery Laboratory, Wakunaga Pharmaceutical Co., Ltd., Akitakata, Hiroshima 739-1195, Japan

ARTICLE INFO

Article history:
Received 10 December 2013
Available online 19 December 2013

Keywords:
Transforming growth factor-β
Liver fibrosis
Hepatic stellate cells
Liver sinusoidal endothelial cells

ABSTRACT

Aim: Hepatic fibrosis and angiogenesis occur in parallel during the progression of liver disease. Fibrosis promotes angiogenesis via inducing vascular endothelial growth factor (VEGF) from the activated hepatic stellate cells (HSCs). In turn, increased neovessel formation causes fibrosis, although the underlying molecular mechanism remains undetermined. In the current study, we aimed to address a role of endothelial cells (ECs) as a source of latent transforming growth factor (TGF)-β, the precursor of the most fibrogenic cytokine TGF-β.

Methods: After recombinant VEGF was administered to mice via the tail vein, hepatic angiogenesis and fibrogenesis were evaluated using immunohistochemical and biochemical analyses in addition to investigation of TGF-β activation using primary cultured HSCs and liver sinusoidal ECs (LSECs).

Results: In addition to increased hepatic levels of CD31 expression, VEGF-treated mice showed increased α-smooth muscle actin (α-SMA) expression, hepatic contents of hydroxyproline, and latency associated protein degradation products, which reflects cell surface activation of TGF-β via plasma kallikrein (PLK). Liberating the PLK-urokinase plasminogen activator receptor complex from the HSC surface by cleaving a tethering phosphatidylinositol linker with its specific phospholipase C inhibited the activating latent TGF-β present in LSEC conditioned medium and subsequent HSC activation.

Conclusion: Neovessel formation (angiogenesis) accelerates liver fibrosis at least in part via provision of latent TGF-β that activated on the surface of HSCs by PLK, thereby resultant active TGF-β stimulates the activation of HSCs.

1. Introduction

Liver fibrosis, a common feature of almost all chronic liver diseases, is caused by the excessive accumulation of extracellular matrix (ECM) proteins, including collagen produced mainly by hepatic stellate cells (HSCs) through the process termed activation [1–3]. Under physiological conditions, quiescent HSCs embrace sinusoids as liver-specific pericytes. When the liver parenchyma is chronically injured by various causes, HSCs detach from the sinusoids and subsequently transform into myofibroblast-like cells. This HSC activation is characterized by a loss of lipid droplets, the enhanced production of ECM, and the expression of activation markers such as α-smooth muscle actin (α-SMA) [4]. The HSC activation process is regulated by both autocrine and paracrine growth factors [4,5], among which transforming growth factor (TGF)-β, the most fibrogenic cytokine, plays a critical role [6,7].

TGF-β is produced as a high molecular weight latent form with its propeptide region known as "latency associated protein (LAP)", and thereby must be activated before exerting its biological activity [8]. Latent TGF-β is activated by plasma kallikrein (PLK), which is bound to glycophosphatidylinositol-anchored urokinase-type plasminogen activator receptor (uPAR) on the cell surface and released by phosphatidylinositol-specific phospholipase C (PI-PLC) [9]. PLK cleaves LAP between R58 and L59 during liver fibrosis [10]. After cleavage, the N-terminal side LAP degradation products ending at R58 (R58 LAP-DPs) remain within the ECM of the liver tissues through LTBP, serving as a footprint for active TGF-β generation. We produced a specific antibody (anti-R58 antibody) that detects a neoepitope at the cutting edge of R58 LAP-DPs [10].

Angiogenesis in the adult liver occurs both in pathological settings, such as cirrhosis and tumor development, and in physiological conditions such as liver regeneration [11,12]. Blood vessels in the liver are classified into the hepatic artery, portal vein and sinusoidal blood vessel groups. Thus, liver sinusoidal endothelial

* Corresponding author. Address: Micro-signaling Regulation Technology Unit, RIKEN Center for Life Science Technologies, 2-1 Hirosawa, Wako, Saitama 351-0198, Japan. Fax: +81 48 462 4675.
E-mail address: skojima@riken.jp (S. Kojima).

0006-291X/$ - see front matter © 2013 Elsevier Inc. All rights reserved.
http://dx.doi.org/10.1016/j.bbrc.2013.12.074

cells (LSECs) are the largest population of endothelial cells in the liver.

Hepatic angiogenesis and fibrogenesis occur in parallel during liver diseases [11,13]. Sahin et al. showed that VEGF transgenic mice with increased serum VEGF concentrations have augmented liver fibrosis [14]. However, how the overproduction of VEGF induces liver fibrosis has not yet been determined.

The current study addressed a role of ECs as a source of latent TGF-β, the precursor of the most fibrogenic cytokine TGF-β.

2. Materials and methods

2.1. Materials

Fluorescein isothiocyanate (FITC)-conjugated rat anti-mouse CD31 monoclonal antibody (Clone 390) and rat anti-mouse CD146 monoclonal antibody (Clone ME-9F1) were purchased from Millipore (Billerica, MA, USA) and Bio Legend (San Diego, CA, USA), respectively. FITC-conjugated mouse anti-α-SMA monoclonal antibody (Clone 1A4) and anti-α-SMA monoclonal antibody (Clone 1A4) were purchased from Sigma–Aldrich (St. Louis, MO, USA) and Dako (Glostrup, Denmark), respectively. Neutralizing mouse anti-TGF-β1 monoclonal antibody (Clone 9016) and sheep anti-rat IgG magnetic bead-conjugated antibody (Cat. No.110-35) were purchased from R&D Systems (Minneapolis, MN, USA) and Invitrogen (Carlsbad, CA, USA), respectively. Recombinant VEGF 165 and PI-PLC were purchased from Santa Cruz Biotechnology (Santa Cruz, CA, USA) and Sigma–Aldrich (St. Louis, MO, USA), respectively. An R58 monoclonal antibody that recognizes neo-epitopes formed via the PLK-dependent proteolytic activation of latent TGF-β1 was produced and characterized as previously reported [10].

2.2. Animal experiments

One hundred microliters of saline with or without recombinant VEGF 165 was injected intravenously via the tail veins of three 10-week-old C57BL/6 male mice (Japan SLC Inc., Shizuoka, Japan) daily at doses of 10 or 20 ng/g body weight for 10 days. The mice were euthanized, and the livers were harvested for biochemical and immunohistochemical analyses. All animal experiments were performed in compliance with the protocols approved by the RIKEN Institutional Animal Use and Care Administrative Advisory Committee.

2.3. Staining of liver tissue sections

Liver tissues were fixed in 4% paraformaldehyde (PFA) and embedded in paraffin, and tissue sections (6-μm thick) were prepared using a Leica sliding microtome (Leica Microsystems, Nussloch, Germany). The liver tissue sections were deparaffinized, rehydrated and incubated for 5 min with a drop of Proteinase K (Dako Envision) in 2 ml of 0.05 M Tris–HCl buffer (pH 7.5) at room temperature. Thereafter, endogenous peroxidase was blocked by incubation with 3% hydrogen peroxide in methanol at room temperature for 10 min. The liver tissue sections were stained with Myer's hematoxylin solution and 1% Eosin Y solution (Muto Pure Chemicals, Tokyo, Japan). For CD31 staining, liver sections were incubated at 4 °C overnight with rat anti-CD31 monoclonal antibody (5 μg/ml) and thereafter with the biotinylated rabbit anti-rat IgG antibody (1:200) included in the Vectastain Elite ABC kit for 30 min at room temperature. A 3,3′-diaminobenzidine (DAB) peroxidase substrate kit (Vector Laboratories, Inc., Burlingame, CA, USA) was used for its chromogenic substrate, which develops as a brown precipitate, to visualize immunolabeling. For α-SMA staining, liver sections were incubated at 4 °C overnight with mouse anti-α-SMA monoclonal antibody (1:100) and thereafter with DAKO Envision's polymer of antibodies labeled with peroxidase for 1 h at room temperature. The DAB peroxidase substrate kit was used for its chromogenic substrate. Sirius red, which results in the red staining of all fibrillary collagen, was used to evaluate fibrosis. The liver sections were stained with 0.05% Fast-green FCF (ChemBlink, Inc., CAS 2353-45-9) and 0.05% Direct red 80 (Polysciences, Inc., CAS 2610-10-18) in saturated picric acid (Muto Pure Chemicals) for 90 min at room temperature. Positive area analyses were performed using the WinROOF image analysis software from 3 randomly selected fields among 3 mice for a total of 9 samples per group.

2.4. Measurement of hepatic hydroxyproline content

The hepatic hydroxyproline content was measured as described by Reddy et al. [15]. Briefly, approximately 40 mg of frozen liver tissue was hydrolyzed in 2 N NaOH for 10 min at 65 °C, followed by incubation at 120 °C for 20 min. The same amount of 6 N HCl was added and incubated at 120 °C for 20 min. Activated charcoal solution (10 mg/ml in 4 N KOH) and 2.2 M acetic acid–0.48 M citric acid buffer (pH 6.5) were added to adjust the pH to 7–8. After centrifugation, 100 mM chloramine T solution was added to the supernatant and incubated at room temperature for 25 min. After the addition of 1 M Ehrlich's solution (*p*-dimethylaminobenzaldehyde), samples were incubated at 65 °C for 20 min. Absorbance was measured at 560 nm. The hydroxyproline content is expressed in μg/mg of sample protein.

2.5. Isolation of HSCs and LSECs

Primary HSCs were isolated from the livers of male C57BL/6 mice by collagenase/pronase digestion and the Nycodenz gradient method as described previously [9]; the cells were then cultured in Dulbecco's modified Eagle's medium (DMEM) containing 10% fetal bovine serum (FBS). Primary LSECs were isolated using a combination of rat anti-CD146 and sheep anti-rat IgG antibodies conjugated with magnetic beads from a fraction separated using the Nycodenz gradient method after the collagenase digestion of the livers of male C57BL/6 mice, according to the method described by Kitazume et al. [16]. The cells were then cultured in a DMEM/nutrient mixture F-12 (F12) containing 10% FBS.

2.6. Preparation of the LSEC conditioned medium (CM)

Briefly, 1×10^5 LSECs were seeded onto 6-well plates and precultured for 24 h with DMEM/F12 containing 10% FBS medium to grow the cells to confluency, followed by overnight starvation with DMEM/F12 containing 2% FBS at 37 °C. After the cells were rinsed with phosphate buffered saline (PBS), the medium was changed to 2 ml of DMEM/F12 containing 2% FBS and further cultured for 24 h to create LSEC CM.

2.7. Immunofluorescent staining

HSCs were fixed with 4% PFA for 10 min and incubated with 0.1% Triton X-100 in PBS for 20 min at room temperature. After blocking with 3% BSA in PBS for 40 min at room temperature, cells were incubated with FITC-conjugated anti-mouse α-SMA monoclonal antibody (1:200) for 2 h at room temperature. After being washed with PBS, the cells were mounted with Vectashield DAPI mounting medium (Vector Laboratories, Inc., Burlingame, CA, USA) and observed under a Zeiss LSM 700 laser scanning confocal microscope. The intensities of α-SMA and R58 LAP-DPs were calculated in each panel with ZEN software for quantitative fluorescence analyses.

2.8. Determination of the TGF-β concentration in CM

TGF-β was measured using a bioassay (luciferase assay in CCL64 cells) for active TGF-β and an enzyme-linked immunosorbent assay (ELISA) for total TGF-β. CCL64 cells, from the mink lung epithelial cell line, stably expressing $(CAGA)_9$-MLP-luciferase, which contains nine copies of an Smad binding CAGA box element upstream of a minimal adenovirus major late promoter [17], were plated at 2×10^4 cells/well in a 96-well plate with DMEM containing 10% FBS. On the next day, the medium was replaced with CM harvested from HSCs. After 6 h, the cells were extracted with a lysis buffer, and luciferase activity was measured using a Luciferase Assay System (Promega, Madison, WI, USA) according to the manufacturer's instructions. The amount of active TGF-β was calculated from a standard curve made with recombinant TGF-β1. The total TGF-β1 levels present in the LSEC CM before and after incubating with HSCs were determined using a TGF-β1 Emax immune Assay System ELISA kit (Promega, Madison, WI, USA) according to the manufacturer's instructions. Samples were acidified using 1 N HCl to a pH of 3.0 for 15–20 min, followed by neutralization with 1 N NaOH before they were subjected to ELISA.

2.9. Real-time RT-PCR

Total RNA isolation and real-time RT-PCR were performed as described previously [18]. Briefly, total RNA was extracted using the RNeasy micro kit (Qiagen, Valencia, CA) according to the manufacturer's protocols. RNA (0.5 μg) was reverse transcribed to

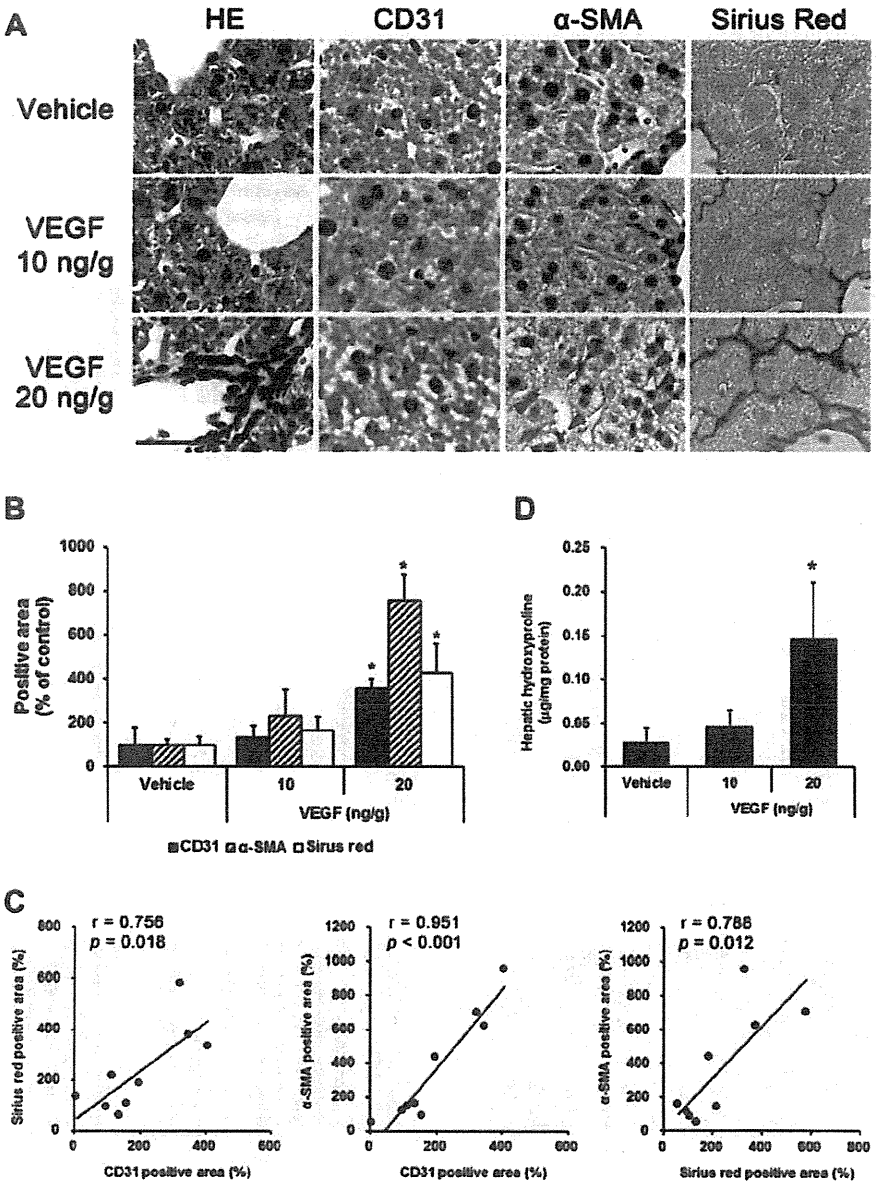

Fig. 1. VEGF simultaneously induced angiogenesis and fibrogenesis in the liver. Saline (100 μl/mouse/day) with or without recombinant VEGF at the indicated doses was injected into the tail vein of three 10-week-old C57BL/6 mice for 10 days. Their livers were removed after the animals were euthanized. (A) Liver tissue sections were prepared and stained with HE, antibodies for CD31 and α-SMA, and Sirius red, as described in the Section 2. Scale bar is 50 μm. Red arrow heads represent α-SMA positive cells. (B) CD31, α-SMA and Sirius red-positive areas (%) were quantitated and plotted as the means ± SD in the bar graphs ($n = 3$). (C) The correlation between CD31 and Sirius red-positive area (left panel), CD31 and α-SMA-positive area (middle panel), and Sirius red- and α-SMA-positive area (right panel). (D) The liver HDP levels were measured as described in the Section 2. *$p < 0.05$ compared with vehicle-treated mice.

cDNA using the PrimeScript® RT Master Mix (Takara Bio Inc., Shiga, Japan). mRNA expression levels were determined using real-time PCR. Real-time PCR was performed with the Thermal Cycler Dice® Real Time System using the SsoAdvanced™ SYBR® Green Supermix (Bio-Rad Laboratories, Hercules, CA) and normalized to 18S rRNA expression. The primer sequences used were as follows: mouse TGF-β1 forward: 5′-GCA ACA ATT CCT GGC GTT ACC-3′, reverse: 5′-CCC TGT ATT CCG TCT CCT TGG T-3′; mouse PLK forward: 5′-GAC CAG AGT ACC GGA AGA AG-3′, reverse: 5′-ACC TAT CTC CGA AAG CGC AC-3′; mouse uPAR forward: 5′-GCC GCT ATC CTA CAG AGC AC-3′, reverse: 5′-GCT ATG GAA ACC TGC TGT GCC-3′; and 18S rRNA forward: 5′-GTA ACC CGT TGA ACC CCA TT-3′, reverse: 5′-CCA TCC AAT CGG TAG TAG CG-3′.

2.10. Statistics

Statistical analyses were performed using one-way analysis of variance, followed by the Dunnett's or Tukey's post hoc tests. A two-tailed Student's *t*-test was used to evaluate the differences between the two groups.

3. Results

3.1. Simultaneous induction of hepatic angiogenesis and fibrogenesis in mice after injection of VEGF

VEGF administration to mice dose-dependently increased the number of cellular infiltrations, endothelial cells (CD31 staining, 3.6-fold at 20 ng VEGF/g of BW), and active HSCs (α-SMA staining, red arrow heads, 7.6-fold at 20 ng VEGF/g of BW), which accompanied an increase in the Sirius red-positive area (4.3-fold at 20 ng VEGF/g of BW) (Fig. 1A and B). Significant correlations were observed among the positive areas of CD31, α-SMA, and Sirius red (Fig. 1C). The hepatic hydroxyproline levels also increased 5-fold at 20 ng VEGF/g of BW (Fig. 1D) and 10-fold at 30 ng VEGF/g of BW (data not shown).

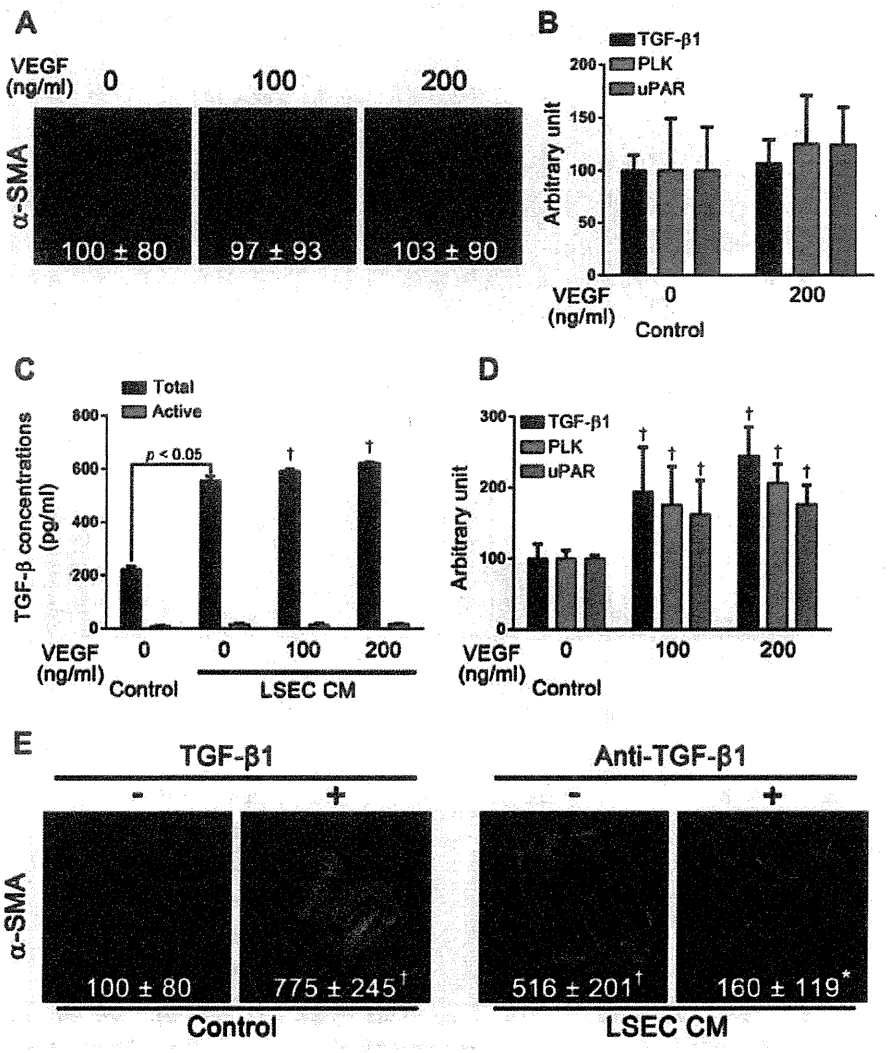

Fig. 2. LSEC CM enhanced HSC activation via TGF-β. Primary HSCs were incubated with 2% FBS DMEM in the presence or absence of the indicated concentrations of recombinant VEGF (A and B), TGF-β1 (100 pg/ml), and LSEC CM in the presence or absence of neutralizing anti-TGF-β1 (2.5 μg/ml) (E) for 5 days. Primary LSECs were incubated with 2% FBS DMEM/F12 in the presence or absence of the indicated concentrations of recombinant VEGF for 24 h (C and D). (A and E) Cells were fixed and stained with α-SMA as described in the Section 2. The relative fluorescence intensities (% of untreated control cells) are shown as the mean ± SD. (B and D) The mRNA expression levels of TGF-β1, PLK, and uPAR were measured using real-time RT-PCR as described in the Section 2. (C) Total/active TGF-β1 levels in the media were measured as described in the Section 2. †$p < 0.05$ compared with untreated control cells, *$p < 0.05$ compared with LSEC CM-treated control cells.

3.2. The enhancement of the activation of HSCs with VEGF-treated LSEC CM via TGF-β

We investigated the molecular mechanism through which VEGF induces hepatic fibrosis in mice using primary cell culture systems. As assessed by the lack of an increase in the α-SMA levels (a marker of activated HSCs), VEGF did not directly activate isolated primary HSCs after 5 days of treatment at 100 and 200 ng/ml, concentrations that are nearly equivalent to the blood concentration of VEGF in in vivo experiments (Fig. 2A). VEGF also did not affect the mRNA expressions of TGF-β1, PLK, and uPAR (Fig. 2B). VEGF enhanced latent TGF-β1 concentration (1.1-fold at 200 ng/ml VEGF) in LSEC CM (Fig. 2C) and mRNA expressions of TGF-β1 (2.4-fold at 200 ng/ml VEGF), PLK (2.1-fold at 200 ng/ml VEGF), and uPAR (1.8-fold at 200 ng/ml VEGF) in LSECs (Fig. 2D). HSCs were activated via incubation with recombinant TGF-β1 (100 pg/ml) and LSEC CM, the latter of which was blocked by incubation with neutralizing antibodies against TGF-β1 (Fig. 2E).

3.3. Latent TGF-β secreted from LSECs is activated by PLK on the surface of HSCs

Given the ELISA and bioassay results, we found that primary LSECs secreted only 2.5% of TGF-β in the active form during 24 h incubation (Fig. 2C), and that the active TGF-β concentrations in LSEC CM were slightly higher than those in the control medium (DMEM containing 2% FBS) (Fig. 2C). To investigate whether latent TGF-β present in LSEC CM was activated by PLK as we previously showed [9], we cultured primary HSCs with LSEC CM with or without PI-PLC, which cleaves the glycophosphatidylinositol anchor, re-

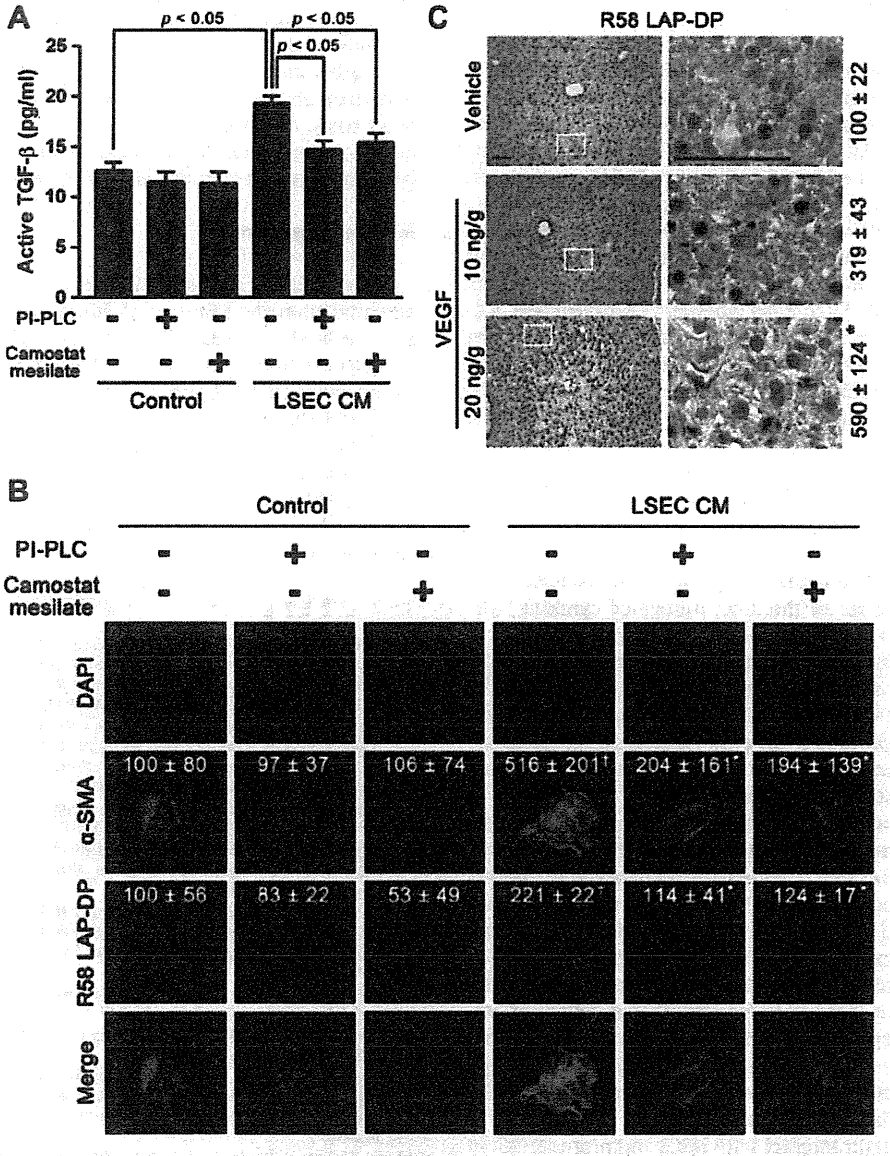

Fig. 3. Latent TGF-β derived from LSECs was activated on the surface of hepatic stellate cells through PLK in in vitro and in vivo. Primary HSCs were incubated with 2% FBS DMEM or LSEC CM in the presence or absence of PI-PLC (0.5 U/mL) or camostat mesilate (500 μM) for 5 days. (A) Active TGF-β1 levels in the media were measured using the luciferase assay in $(CAGA)_9$-Luc CCL64 cells. Data are shown as the means ± SD. (B) Cells were fixed and stained with α-SMA and R58 LAP-DPs as described in the Section 2. The relative fluorescence intensities (% of untreated control cells) are shown as the means ± SD. (C) The liver sections harvested from the VEGF-injected mice were stained with anti-R58 LAP-DPs antibody, as described in the Section 2. The right panels show higher magnifications of the corresponding white squares in the left panels. Scale bars, 100 μm. Positive areas (%) were quantitated and shown as the means ± SD ($n = 3$). †$p < 0.05$ compared with untreated control cells, *$p < 0.05$ compared with LSEC CM-treated control cells.

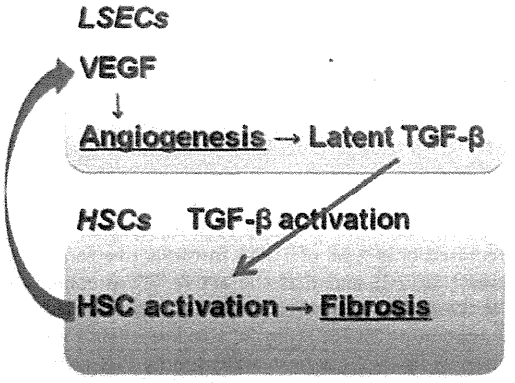

Fig. 4. The scheme of the molecular mechanism through which angiogenesis promotes fibrosis in the liver. Increased neovessels provided with latent TGF-β, which PLK activates on the surface of HSCs and stimulates the activation of HSCs. Therefore, angiogenesis might accelerate liver fibrosis.

leases uPAR and its associated with PLK from the cell surface, or with or without camostat mesilate, a serine protease inhibitor. Both these treatments resulted in a reduction in the concentration of active TGF-β in the LSEC CM (Fig. 3A). LSEC CM failed to activate the HSCs that had been incubated with either PI-PLC or camostat mesilate (Fig. 3B). The R58 LAP-DP levels, a footprint of PLK-dependent TGF-β activation [9], were reduced via either PI-PLC or camostat mesilate. VEGF did not affect R58 LAP-DPs expression (Relative fluorescent intensity: Control 100 ± 56; VEGF 100 ng/ml 112 ± 30; VEGF 200 ng/ml 99 ± 48). To confirm whether PLK-dependent activation might be increased along with neovessel formation in vivo, the liver sections harvested from the VEGF-administered mice were stained with anti-R58 LAP-DPs antibody. As expected, the R58-positive area was increased with VEGF injection by 5.9-fold (Fig. 3C).

4. Discussion

In the present study, we addressed a role of ECs as a source of latent TGF-β, the precursor of the most fibrogenic cytokine TGF-β. We provided in vitro evidence that LSEC CM promotes the activation of quiescent HSCs via the provision of latent TGF-β and in vivo evidence that much more severe fibrosis was induced in the livers of mice that received VEGF (Fig. 4). These data suggest that HSC activation is promoted not only via changes in the extracellular matrix, inflammatory cytokines, and oxidative stress but also secondarily via pathological angiogenesis.

We documented that TGF-β, which is secreted from LSECs as a latent form and activated on the surface of mainly HSCs rather than LSECs (compare Figs. 3A and 2C), mediates enhancement in liver fibrosis, although the expressions of PLK and uPAR increased 2-fold in VEGF-treated LSECs (Fig. 2D). Several groups have reported that VEGF enhanced the expression of urokinase-type plasminogen activator and its receptor uPAR in both bovine microvascular endothelial cells and human umbilical vein endothelial cells [19], enabling them matrix degradation and cell invasion [20], and that bradykinin production via the PLK-dependent cleavage of high molecular weight kininogen promotes angiogenesis via the upregulation of basic fibroblast growth factor [21]. In our study, increased PLK in LSECs might interact with HSCs and promote TGF-β activation on the surface of HSCs. At the same time, increased uPAR and PLK in LSECs also might contribute to angiogenesis. We showed that VEGF increased the levels of hepatic CD31 by 3.6-fold and R58 LAP-DPs by 5.9-fold in mice and that VEGF enhanced latent TGF-β production and TGF-β1 mRNA expression in primary LSECs. These data also suggest that LSECs serve as the source of TGF-β for liver fibrosis.

Yoshiji et al. demonstrated that VEGF receptor expression increased in HSCs along with the development of fibrosis and that a neutralizing anti-VEGF receptor antibody attenuated both angiogenesis and fibrogenesis in the liver [22], using activated HSCs, whereas we used quiescent HSCs. The result in Fig. 1 suggests that VEGF promotes the growth of LSECs, which appears to serve as a source of latent TGF-β, thereby increasing the hepatic levels of TGF-β1, due to the increased number of LSECs in the early stages of liver fibrosis (Fig. 4). Eventually, HSCs were activated and began to express the VEGF receptor, respond to VEGF, and transition to a more activated state. However, we cannot rule out the involvement of other soluble factors, such as PDGF, which is also produced from LSECs and stimulates HSC activation [11,23].

Sorafenib, a multikinase inhibitor recently approved to treat unresectable hepatocellular carcinoma, was beneficial in a model of BDL-induced cirrhosis [24,25]. We have provided here evidence that angiogenesis accelerates liver fibrosis. The anti-fibrotic effect of sorafenib might be caused by its blocking of angiogenesis. Moreover, other anti-angiogenic treatments such as vatalanib [26] and bevacizumab [27], are now being evaluated in clinical cancer treatment trials. An implication of the current study is that anti-angiogenic agents such as vatalanib and bevacizumab might be beneficial for anti-fibrotic therapy in addition to sorafenib.

Acknowledgments

This work was supported in part by a Grant-in-Aid for Scientific Research from the Ministry of Education, Culture, Sports, Science and Technology (23390202 to S.K.), Grants for Collaborative Researchers from Industries (to K.S.), the Uehara Memorial Foundation, Japan (to S.K.), and the Research on the Innovative Development and the Practical Application of New Drugs for Hepatitis B (Principal investigator: Soichi Kojima; H24-B Drug Discovery-Hepatitis-General-003) provided by the Ministry of Health, Labor and Welfare of Japan.

References

[1] S.L. Friedman, Mechanisms of hepatic fibrogenesis, Gastroenterology 134 (2008) 1655–1669.
[2] R. Bataller, D.A. Brenner, Liver fibrosis, J. Clin. Invest. 115 (2005) 209–218.
[3] N.C. Henderson, T.D. Arnold, Y. Katamura, M.M. Giacomini, J.D. Rodriguez, J.H. McCarty, A. Pellicoro, E. Raschperger, C. Betsholtz, P.G. Ruminski, D.W. Griggs, M.J. Prinsen, J.J. Maher, J.P. Iredale, A. Lacy-Hulbert, R.H. Adams, D. Sheppard, Targeting of αv integrin identifies a core molecular pathway that regulates fibrosis in several organs, Nat. Med. 19 (2013) 1617–1624.
[4] S.L. Friedman, Hepatic stellate cells: protean, multifunctional, and enigmatic cells of the liver, Physiol. Rev. 88 (2008) 125–172.
[5] H. Tsukamoto, Cytokine regulation of hepatic stellate cells in liver fibrosis, Alcohol. Clin. Exp. Res. 23 (1999) 911–916.
[6] F.R. Weiner, M.A. Giambrone, M.J. Czaja, A. Shah, G. Annoni, S. Takahashi, M. Eghbali, M.A. Zern, Ito-cell gene expression and collagen regulation, Hepatology 11 (1990) 111–117.
[7] M. Matsuoka, N.T. Pham, H. Tsukamoto, Differential effects of interleukin-1α, tumor necrosis factor α, and transforming growth factor β1 on cell proliferation and collagen formation by cultured fat-storing cells, Liver 9 (1989) 71–78.
[8] S.B. Jakowlew, J.E. Mead, D. Danielpour, J. Wu, A.B. Roberts, N. Fausto, Transforming growth factor-β (TGF-β) isoforms in rat liver regeneration: messenger RNA expression and activation of latent TGF-β, Cell Regul. 2 (1991) 535–548.
[9] K. Akita, M. Okuno, M. Enya, S. Imai, H. Moriwaki, N. Kawada, Y. Suzuki, S. Kojima, Impaired liver regeneration in mice by lipopolysaccharide via TNF-α/kallikrein-mediated activation of latent TGF-β, Gastroenterology 123 (2002) 352–364.
[10] S. Kojima, Detection of hepatic fibrogenesis targeting proteolytic TGF-β activation reaction, Hepatology (2008) 917A.
[11] D. Thabut, V. Shah, Intrahepatic angiogenesis and sinusoidal remodeling in chronic liver disease: new targets for the treatment of portal hypertension?, J Hepatol. 53 (2010) 976–980.
[12] B.S. Ding, D.J. Nolan, J.M. Butler, D. James, A.O. Babazadeh, Z. Rosenwaks, V. Mittal, H. Kobayashi, K. Shido, D. Lyden, T.N. Sato, S.Y. Rabbany, S. Rafii,

Inductive angiocrine signals from sinusoidal endothelium are required for liver regeneration, Nature 468 (2010) 310–315.
[13] M. Fernandez, D. Semela, J. Bruix, I. Colle, M. Pinzani, J. Bosch, Angiogenesis in liver disease, J. Hepatol. 50 (2009) 604–620.
[14] H. Sahin, E. Borkham-Kamphorst, C. Kuppe, M.M. Zaldivar, C. Grouls, M. Al-samman, A. Nellen, P. Schmitz, D. Heinrichs, M.L. Berres, D. Doleschel, D. Scholten, R. Weiskirchen, M.J. Moeller, F. Kiessling, C. Trautwein, H.E. Wasmuth, Chemokine Cxcl9 attenuates liver fibrosis-associated angiogenesis in mice, Hepatology 55 (2012) 1610–1619.
[15] G.K. Reddy, C.S. Enwemeka, A simplified method for the analysis of hydroxyproline in biological tissues, Clin. Biochem. 29 (1996) 225–229.
[16] S. Kitazume, R. Imamaki, K. Ogawa, Y. Komi, S. Futakawa, S. Kojima, Y. Hashimoto, J.D. Marth, J.C. Paulson, N. Taniguchi, α2,6-sialic acid on platelet endothelial cell adhesion molecule (PECAM) regulates its homophilic interactions and downstream antiapoptotic signaling, J. Biol. Chem. 285 (2010) 6515–6521.
[17] P.K. Datta, H.L. Moses, STRAP and Smad7 synergize in the inhibition of transforming growth factor β signaling, Mol. Cell. Biol. 20 (2000) 3157–3167.
[18] K. Sakata, M. Hara, T. Terada, N. Watanabe, D. Takaya, S. Yaguchi, T. Matsumoto, T. Matsuura, M. Shirouzu, S. Yokoyama, T. Yamaguchi, K. Miyazawa, H. Aizaki, T. Suzuki, T. Wakita, M. Imoto, S. Kojima, HCV NS3 protease enhances liver fibrosis via binding to and activating TGF-β type I receptor, Sci. Rep. 3 (2013) 3243.
[19] S.J. Mandriota, G. Seghezzi, J.D. Vassalli, N. Ferrara, S. Wasi, R. Mazzieri, P. Mignatti, M.S. Pepper, Vascular endothelial growth factor increases urokinase receptor expression in vascular endothelial cells, J. Biol. Chem. 270 (1995) 9709–9716.
[20] J.M. Breuss, P. Uhrin, VEGF-initiated angiogenesis and the uPA/uPAR system, Cell Adh. Migr. 6 (2012) 535–615.
[21] R.W. Colman, Regulation of angiogenesis by the kallikrein–kinin system, Curr. Pharm. Des. 12 (2006) 2599–2607.
[22] H. Yoshiji, S. Kuriyama, J. Yoshii, Y. Ikenaka, R. Noguchi, D.J. Hicklin, Y. Wu, K. Yanase, T. Namisaki, M. Yamazaki, H. Tsujinoue, H. Imazu, T. Masaki, H. Fukui, Vascular endothelial growth factor and receptor interaction is a prerequisite for murine hepatic fibrogenesis, Gut 52 (2003) 1347–1354.
[23] J.S. Lee, D. Semela, J. Iredale, V.H. Shah, Sinusoidal remodeling and angiogenesis: a new function for the liver-specific pericyte?, Hepatology 45 (2007) 817–825
[24] D. Thabut, C. Routray, G. Lomberk, U. Shergill, K. Glaser, R. Huebert, L. Patel, T. Masyuk, B. Blechacz, A. Vercnocke, E. Ritman, R. Ehman, R. Urrutia, V. Shah, Complementary vascular and matrix regulatory pathways underlie the beneficial mechanism of action of sorafenib in liver fibrosis, Hepatology 54 (2011) 573–585.
[25] M. Mejias, E. Garcia-Pras, C. Tiani, R. Miquel, J. Bosch, M. Fernandez, Beneficial effects of sorafenib on splanchnic, intrahepatic, and portocollateral circulations in portal hypertensive and cirrhotic rats, Hepatology 49 (2009) 1245–1256.
[26] J.M. Wood, G. Bold, E. Buchdunger, R. Cozens, S. Ferrari, J. Frei, F. Hofmann, J. Mestan, H. Mett, T. O'Reilly, E. Persohn, J. Rosel, C. Schnell, D. Stover, A. Theuer, H. Towbin, F. Wenger, K. Woods-Cook, A. Menrad, G. Siemeister, M. Schirner, K.H. Thierauch, M.R. Schneider, J. Drevs, G. Martiny-Baron, F. Totzke, PTK787/ZK 222584, a novel and potent inhibitor of vascular endothelial growth factor receptor tyrosine kinases, impairs vascular endothelial growth factor-induced responses and tumor growth after oral administration, Cancer Res. 60 (2000) 2178–2189.
[27] N. Ferrara, K.J. Hillan, H.P. Gerber, W. Novotny, Discovery and development of bevacizumab, an anti-VEGF antibody for treating cancer, Nat. Rev. Drug. Discovery 3 (2004) 391–400.

Liver INTERNATIONAL
OFFICIAL JOURNAL OF THE INTERNATIONAL ASSOCIATION FOR THE STUDY OF THE LIVER

Liver International ISSN 1478-3223

VIRAL HEPATITIS

Hepatic stellate cells that coexpress LRAT and CRBP-1 partially contribute to portal fibrogenesis in patients with human viral hepatitis

Keisuke Nagatsuma[1,2], Hiroshi Hano[2], Kazuhiro Murakami[3], Daisuke Shindo[4], Yoshihiro Matsumoto[1], Jimi Mitobe[1,2], Ken Tanaka[1], Masaya Saito[5], Haruka Maehashi[4], Mamiko Owada[2], Masahiro Ikegami[2], Akihito Tsubota[6], Toshifumi Ohkusa[7], Yoshio Aizawa[8], Ichiro Takagi[1], Hisao Tajiri[1] and Tomokazu Matsuura[1,4]

1 Division of Gastroenterology and Hepatology, Department of Internal Medicine, The Jikei University School of Medicine, Tokyo, Japan
2 Department of Pathology, The Jikei University School of Medicine, Tokyo, Japan
3 Division of Clinical Pathology, Tohoku Welfare Pension Hospital, Sendai, Japan
4 Department of Laboratory Medicine, The Jikei University School of Medicine, Tokyo, Japan
5 Kaijo Bldg. Clinic, Tokyo, Japan
6 Institute of Clinical Medicine and Research (ICMR), The Jikei University School of Medicine, Chiba, Japan
7 Division of Gastroenterology and Hepatology, Kashiwa Hospital, The Jikei University School of Medicine, Chiba, Japan
8 Division of Gastroenterology and Hepatology, Katsushika Medical Centre, The Jikei University School of Medicine, Tokyo, Japan

Keywords
Cellular retinol-binding protein-1 (CRBP-1) – hepatic stellate (Ito) cell (HSC) – lecithin retinol acyltransferase (LRAT) – portal fibrosis – retinoid(vitamin A)

Correspondence
Tomokazu Matsuura, MD., PhD., Department of Laboratory Medicine, The Jikei University School of Medicine, 3-25-8 Nishi-shimbashi, Minato-ku, Tokyo 105-8461, Japan
Tel: +81 3 3433 1111 (ext 3210)
Fax: +81 3 3437 5560
e-mail: matsuurat@jikei.ac.jp

Received 17 December 2012
Accepted 12 June 2013

DOI:10.1111/liv.12255
Liver Int. 2014: 34: 243–252

Abstract

Background & Aims: Precisely what type of cells mainly contributes to portal fibrosis, especially in chronic viral hepatitis, such as hepatic stellate cells (HSCs) in the parenchyma or myofibroblasts in the portal area, still remains unclear. It is necessary to clarify the characteristics of cells that contribute to portal fibrosis in order to determine the mechanism of portal fibrogenesis and to develop a therapeutic target for portal fibrosis. This study was undertaken to examine whether LRAT+/CRBP-1+ HSCs contribute to portal fibrosis on viral hepatitis. *Methods:* Antibodies to lecithin:retinol acyltransferase (LRAT), cellular retinol-binding protein-1 (CRBP-1) and widely ascertained antibodies to HSCs (alpha-smooth muscle actin, neurotrophin-3) and endothelial cells (CD31) were used for immunohistochemical studies to assess the distribution of cells that contribute to the development of portal fibrosis with the aid of fluorescence microscopy. A quantitative analysis of LRAT+/CRBP-1+ HSCs was performed. *Results:* The number of LRAT+/CRBP-1+ HSCs was increased in fibrotic liver in comparison with normal liver in the portal area and fibrous septa. The number of double positive cells was less than 20% of all cells/field in maximum. *Conclusion:* This study provides evidence that functional HSCs coexpressing both LRAT and CRBP-1 that continue to maintain the ability to store vitamin A contribute in part to the development of portal fibrogenesis in addition to parenchymal fibrogenesis in patients with viral hepatitis.

Hepatic stellate cells (HSCs), also referred to as Ito cells or fat-storing cells, have been regarded as essential cells for liver fibrogenesis. In a normal liver, HSCs store 80–90% of the hepatic retinoid in characteristic lipid droplets as *fat-storing cells*. When activated in the presence of liver damage, HSCs release cytokines, primarily TGF-β, and transform into myofibroblasts lacking fat droplets. They then produce excessive extracellular matrix and disrupt the liver cytoarchitecture, eventually leading to cirrhosis and liver failure (1).

Hepatic myofibroblasts are transdifferentiated from heterogeneous cell populations in response to a variety of fibrogenic stimuli. Recently, there have been reports that the cellular origin of fibrogenic myofibroblasts is HSCs, portal fibroblasts (6), other mesenchymal cells (6, 7), bone marrow cells (2–5), epithelial-like cells such as hepatocytes or cholangiocytes (8–11) and endothelial cells (12). Although these reports are credible, it is unclear whether this cellular transformation occurs in actual human liver diseases. The current consensus is that hepatic myofibroblasts, myofibroblasts generated in parenchymal injury appear to originate from HSCs and myofibroblasts generated in portal injury may originate from portal fibroblasts (13). However, most of these results were obtained using cultured cells or rodent models. There are few reports that examined the origin

of myofibroblasts in actual human liver diseases, especially in portal injury. Therefore, it is important to determine which type of cells contributes to portal fibrosis in human diseased livers.

One of the candidates that can serve as a marker of quiescent HSCs, which store retinoids in the space of Disse, is lecithin:retinol acyltransferase (LRAT). LRAT activity is strongly expressed in the liver, retinal pigment epithelial (RPE) cells, intestinal mucosa, basal keratinocytes, testis, lungs, *etc.* LRAT has been defined to play the following roles: storing systemic retinoid in the liver, incorporating retinol into the retina and adjusting its concentration in the retinal pigment epithelium to maintain visual function, adjusting the regional concentration of retinoid to differentiate the epithelium in the skin and lungs and regulating the concentration of retinoid to maintain a level optimal for maturation of spermatozoa in the testis (14–20).

Lecithin retinol acyltransferase is also the physiological retinol esterification enzyme which stores retinoid in the liver. Retinyl esters are biosynthesized by removing the fatty acid at position sn-1 of lecithin, using cellular retinol-binding protein-1 (CRBP-1)-bound retinol as a substrate. The expression of LRAT in the liver is regulated by the vitamin A status. Whereas hepatic LRAT activity is low in the livers of vitamin A deficient rats, the decreased LRAT activity is rapidly elevated by repletion with retinol, retinoic acid or RAR-agonists (21–23). Furthermore, LRAT activity is higher in the non-parenchymal cell fraction than in the hepatocyte fraction, and it is estimated that in the liver, the LRAT activity is specifically distributed in HSCs (15). We previously generated antimouse and antihuman LRAT antibodies using peptides of the amino acid sequence of mouse hepatic LRAT and human RPE LRAT, respectively, and reported that these proteins were expressed in quiescent HSCs and endothelial cells of rodent and human normal livers (24).

Cellular retinol-binding protein-1, one of retinol-binding proteins, is present in a variety of tissues, and is most highly expressed in the liver, kidneys and proximal epididymis (25, 26). CRBP-1 is highly expressed in the liver: hepatocytes account for more than 90% of hepatic CRBP-1, while the concentration of the protein (per protein unit) in HSCs is 22 times greater than in hepatocytes (27). In the liver, CRBP-1 mediates retinol esterification to retinyl esters (28). CRBP1-bound retinol is also the substrate of LRAT (29) and the interaction between LRAT and CRBP-1 is required for this enzymatic reaction (30). In an immunohistochemical study, it was shown that quiescent rat HSCs express CRBP-1 (31–33) and quiescent HSCs and myofibroblasts in human normal and diseased livers also express CRBP-1, in addition to hepatocytes and cholangiocytes express CRBP-1 (34, 35).

As described above, both LRAT and CRBP-1 are key molecules involved in the retinoid metabolism in the liver, and in this work we regarded cells coexpressing LRAT and CRBP-1 as functional HSCs that have the ability to store vitamin A.

In this study, the *in situ* distribution of functional HSCs that expressed both LRAT and CRBP-1 was examined in human normal and pathological livers, particularly livers of patients with hepatitis C and B, in order to clarify the contribution of HSCs to portal fibrosis.

Materials and methods

Human liver specimens

Human liver samples were obtained from 24 patients. They corresponded either to percutaneous liver biopsies (n = 20) or large surgical specimens (n = 4). Four corresponded to histologically normal livers and 20 to pathological specimens (Table. 1) with various fibrotic stages. Non-tumourous areas in specimens resected for liver metastasis of colon cancer and in specimens of haemangioma of the liver were studied as histologically 'normal' livers. The stage of fibrosis and the grade of inflammatory activity were classified according to the METAVIR score (36). This work was performed with the permission of the Ethics Committee for Biomedical Research of the Jikei University School of Medicine.

Table 1. Pathological specimens

	Age	Sex	Fibrosis*	Activity†	Aetiology
1	43	F	F0	A0	Metastatic liver tumor
2	60	F	F0	A0	Metastatic liver tumor
3	35	F	F0	A0	Liver hemangioma
4	83	F	F0	A0	Metastatic liver tumor
5	55	M	F1	A1	HCV
6	63	F	F1	A2	HCV
7	52	F	F1	A1	HCV
8	25	M	F1	A1	HBV
9	51	F	F1	A2	HBV
10	58	F	F2	A3	HCV
11	51	F	F2	A2	HCV
12	62	M	F2	A2	HBV
13	40	M	F2	A2	HBV
14	63	M	F2	A1	HCV
15	55	M	F3	A1	HCV
16	36	M	F3	A3	HBV
17	40	M	F3	A2	HBV
18	28	M	F3	A2	HBV
19	64	F	F3	A2	HCV
20	39	M	F4	A2	HCV
21	47	M	F4	A3	HCV
22	72	M	F4	A2	HCV
23	57	M	F4	A1	HBV
24	70	M	F4	A2	HCV

HBV, hepatitis B virus; HCV, hepatitis C virus.

*F0, no fibrosis; F1, portal fibrosis without septa; F2, portal fibrosis with rare septa; F3, numerous septa without cirrhosis; F4, cirrhosis.

†A0, no activity; A1, mild activity; A2, moderate activity; A3, severe activity. No. 1-4: non-tumourous area in the livers with metastasis or haemangioma.

Tissue sampling and processing

A portion of the fresh tissue samples was routinely utilized to prepare 10% buffered neutral formalin-fixed and paraffin-embedded sections for liver pathology diagnosis; these samples were also used for this study. Three micrometer-thick paraffin sections of each sample were stained with haematoxylin-eosin, Masson's trichrome and silver impregnation for the diagnostic purposes.

Antibodies, immunostaining and observation

An antibody specific for human RPE LRAT (Immuno-Biological Laboratories, Gunma, Japan), a rabbit polyclonal antibody against human cellular retinol-binding protein-1 (CRBP-1) (FL-135) (sc-30106; Santa Cruz Biotechnology, Inc., California, CA, USA), a mouse monoclonal antibody against human smooth muscle actin (SMA) (IgG2a) (Clone 1A4; Dako A/S, Denmark), a rabbit polyclonal antibody against neurotrophin-3 (NT-3) (N-20) (sc-547; Santa Cruz Biotechnology, Inc., California, CA, USA) and a mouse monoclonal antibody against CD31 (IgG1, kappa) (Clone JC70A; Dako A/S, Denmark) were used for the immunohistochemical studies.

The formalin-fixed specimens were embedded in paraffin, and 3 μm-thick sections were cut for immunohistochemical examination. After deparaffinization, the sections of human liver were microwave-treated in 10 mM citrate buffer (pH 6.0) for 10 min at 95°C to activate the antigens, then samples were allowed to cool at room temperature for 15 min. The sections were then rinsed with PBS, and endogeneous peroxidase was inhibited by 0.3% hydrogen peroxide in methanol for 30 min at room temperature. After blocking the samples with 5% goat whole serum (Immuno-Biological Laboratories)/PBS, the sections were incubated with antibodies diluted in PBS against human LRAT (1:20), human CRBP-1 (1:50), human SMA (1:500) and human NT-3 (1:50) for 60 min at room temperature. The sections were then rinsed in PBS, and the epitopes were detected with the Envision + system by horseradish peroxidase detection of antirabbit or antimouse (Dako, Carpinteria, CA, USA) for 60 min at room temperature. The immunoreaction was visualized by using 0.5% 3, 3′-diam-

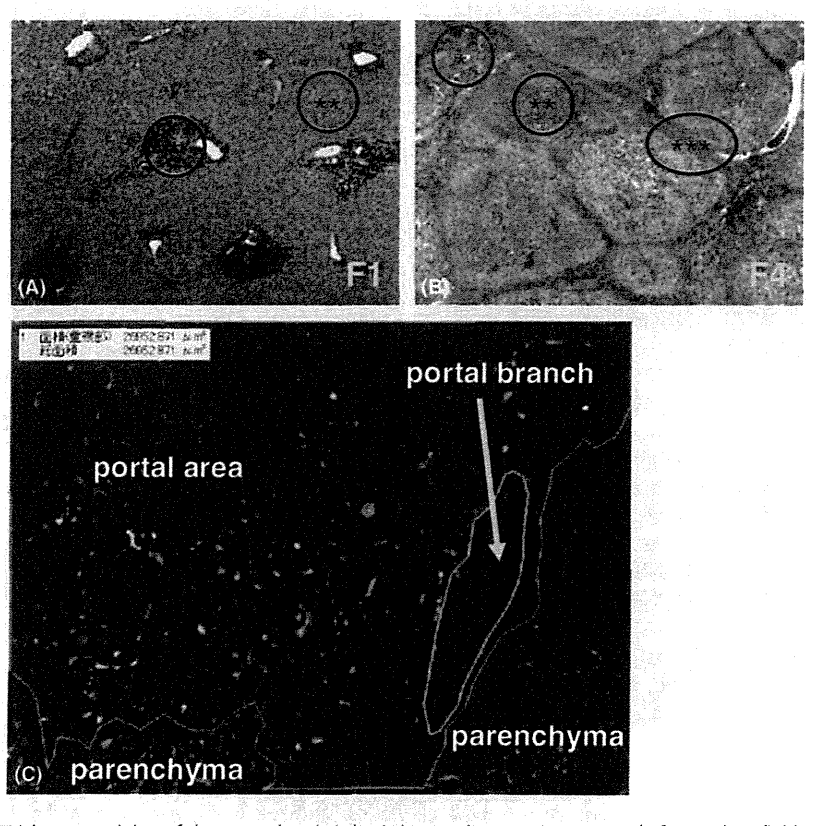

Fig. 1. (A, B): Masson-Trichrome staining of the normal and cirrhotic human liver sections. A total of 3 random fields each in the parenchyma, portal area and fibrous septa (only F3, F4) were used for the quantitative analysis of each case. *portal area, **parenchyma, ***fibrous septa (C) Double immunofluorescence staining for LRAT (green labelling) and CRBP-1 (red labelling) of human liver sections. Each area was automatically measured using a VH analyzer, using the Keyence software program for quantitative analysis, according to the formula: all field - (parenchyma area + portal branch area) = portal area.

inobenzidine tetrahydrochloride (DAB; Dojinkagaku, Japan) and 0.1% hydrogen peroxide in 50 mM Tris buffer (pH 7.6) at room temperature. The sections were lightly washed, counterstained with haematoxylin, dehydrated in ethanol and mounted with Permount.

For double immunostaining of LRAT/SMA, LRAT/CD31 and LRAT/CRBP-1, a Ventana XT System Benchmark (Ventana Medical Systems, Inc., Tucson, AZ, USA) (automated immunohistochemical instrument) was used. Double immunostaining was performed using antibodies at the same dilutions as described above except for CD31 (1:20). The immunoreaction was visualized by using an i-View DAB and RED detection kit (Ventana Medical Systems, Inc.) for each antibody.

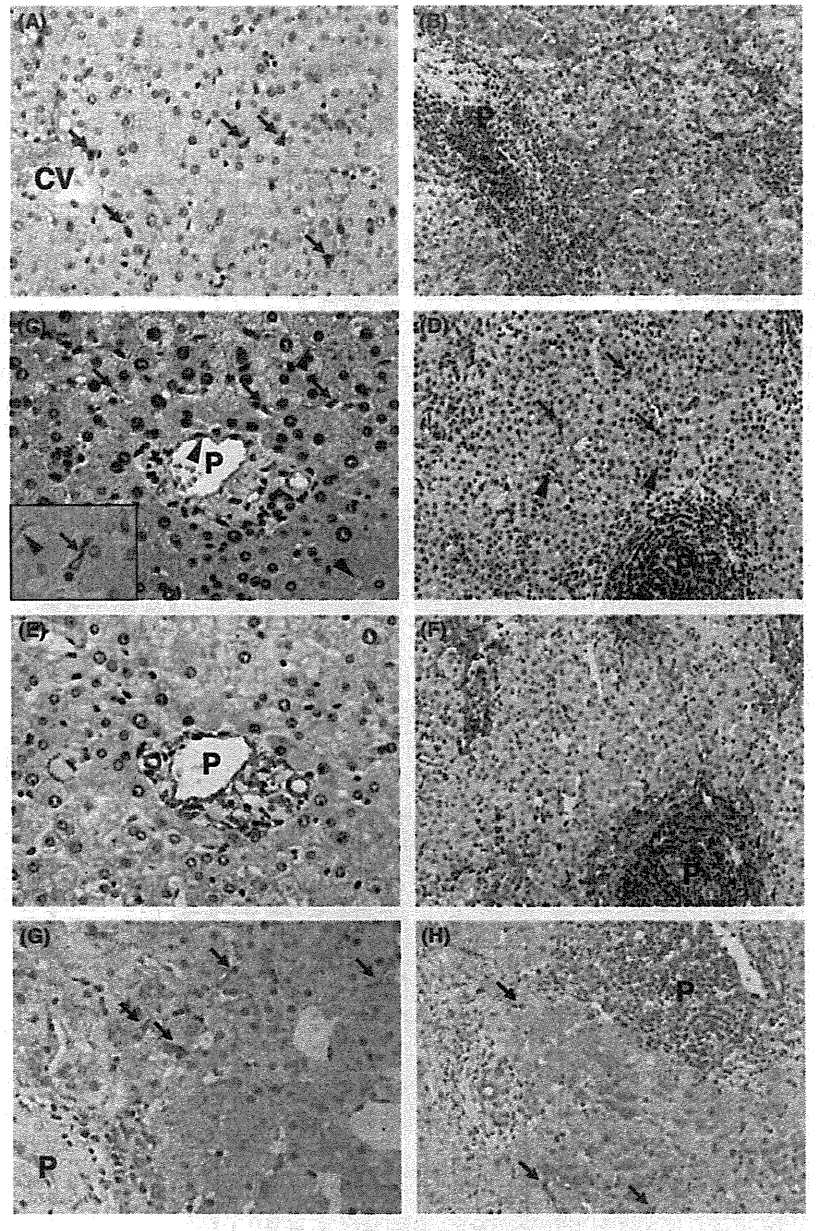

Fig. 2. Immunostaining of normal METAVIR score F0A0 (A, C, E, G) and fibrotic METAVIR score F2A2 (B, D, F, H) human liver sections. (A, B): Liver sections stained for CRBP-1 showed that HSCs (arrows) were positively stained in normal and fibrotic liver. (C, D): Liver sections stained for LRAT showed that both HSCs (arrows) and endothelial cells (arrowheads) were positively stained in the normal and fibrotic liver. The inset shows a higher magnification view of a HSC. (E, F): Liver sections stained for smooth muscle actin (SMA) showed that the HSCs in the space of Disse were hardly stained, while the myofibroblasts around the portal area and smooth muscle cells in small arteries in the portal area were positively stained. (G, H): Liver sections stained for neurotrophin-3 (NT-3) showed that HSCs (arrows) were positively stained in the normal and fibrotic liver. (CV; central vein, P; portal vein) magnification: A, C, E, G; ×200, B, D, F, H; ×100, C (inset); ×1,000.

Subsequently, double immunofluorescence staining was evaluated. After antigen retrieval using a microwave, the sections were incubated with the mixture of anti-LRAT antibody labelled with FITC (Invitrogen Corporation, Carlsbad, CA, USA) and anti-CRBP-1 antibody labelled with R-Phycoerythrin (Seikagaku Biobusiness Corporation, Tokyo, Japan) at the same dilutions as described previously for 60 min at room temperature. The sections were lightly washed and mounted with ProLong® Gold antifade reagent (Molecular Probes, Eugene, OR, USA). As a negative control, we used Negative Control Rabbit IgG (Biocare Medical, Concord, CA, USA) at the same concentration as the respective antibodies.

Finally, sections were examined by fluorescence microscopy using a Biozero BZ-8000 microscope (Keyence Corporation, Osaka, Japan).

Quantitative evaluation of LRAT and CRBP-1 double positive hepatic stellate cells

Quantitative evaluation of double immunofluorescence was performed using a fluorescence microscope (Biozero BZ-8000; Keyence Corporation, Osaka, Japan). After double immunofluorescence staining, the number of LRAT+/CRBP-1+ cells/field was counted in 3 random fields each in the parenchyma, portal area and fibrous septa (only F3, F4) in each case. Each area was automatically measured using a VH analyzer (Keyence Corporation, Osaka, Japan). The average number of LRAT+/CRBP-1+ cells/field was calculated in F0-F4 respectively (Fig. 1).

Statistical analysis

Comparisons between the two groups were performed using Student's *t*-test. The difference between groups was considered statistically significant at $P < 0.05$.

Results

Immunohistochemical examination of liver specimens

Human liver samples obtained from 24 patients were studied. The samples were from 10 females and 14 males aged 25–83 years (average: 52 years). Livers of various fibrotic stages were classified into F1–F4 according to their METAVIR score, excluding normal livers. The cases of viral hepatitis or cirrhosis were used as pathological liver specimens in order to demonstrate whether HSCs were present in the fibrotic areas around the central vein but also in portal fibrosis.

Human normal and fibrotic liver specimens were immunostained with anti-CRBP-1, anti-LRAT, anti-SMA and anti-NT-3 antibodies. HSCs in the space of Disse were positively stained for both CRBP-1 and LRAT in the normal and fibrotic liver specimens (Fig. 2A–D). In addition, the endothelial cells of the portal vein and sinusoids were stained with the anti-LRAT antibody (Fig. 2C,D). Smooth muscle actin (SMA), an actin isoform, can be regarded as a good marker for identification of activated HSCs (37). HSCs in the space of Disse were barely stained for SMA, in contrast to the CRBP-1 and LRAT staining, although the myofibroblasts in the portal area and fibrous fascicles were positively stained (Fig. 2E,F). NT-3, a neurotrophic factor, is also regarded to be a marker identifying HSCs (38, 39). In this study, HSCs in the space of Disse were positively stained for NT-3, as well as LRAT and CRBP-1, in the normal and fibrotic liver specimens (Fig. 2G,H).

Double immunostaining for LRAT and SMA in human cirrhotic liver specimens showed that SMA was

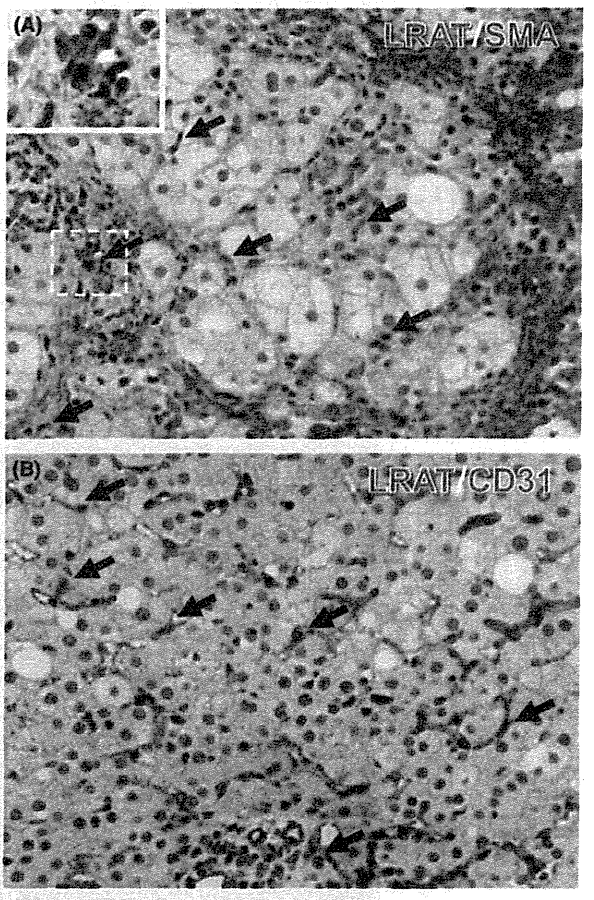

Fig. 3. (A) Double immunostaining for LRAT (brown labelling) and SMA (red labelling) of human cirrhotic liver (METAVIR score of F4A2). SMA was positive in the fibrous fascicles. On the other hand, a few LRAT positive cells (arrows) were observed in the parenchyma and fibrous septa. The inset shows a higher magnification view of a HSC which colocalizated with LRAT and SMA in fibrous fascicles. (B) Double immunostaining for LRAT (brown labelling) and CD31 (red labelling) of the human liver (METAVIR score of F1A1). CD31 was positive in endothelial cells in the sinusoid and portal area. LRAT was positive in both HSCs (arrows) and endothelial cells in the sinusoid. magnification: ×200, inset×1000.

strongly positive in fibrous fascicles, while LRAT was mainly positive in HSCs in the space of Disse. Some of the LRAT positive cells in the fibrous fascicles were co-localizated with SMA positive cells (Fig. 3A). Double immunostaining for LRAT and CD31 in the human liver specimens revealed positivity for CD31 in endothelial cells in the sinusoid and portal area and positivity for LRAT in both HSCs (arrows) and endothelial cells in the sinusoid (Fig. 3B).

Double immunostaining for LRAT and CRBP-1 in the human liver specimens showed LRAT+/CRBP-1+ cells in HSCs in the parenchyma (arrows) and myofibroblasts in the portal area (arrowheads) (Fig. 4A). The double immunofluorescence staining for LRAT and CRBP-1 in the human fibrotic liver detected by fluorescence microscopy showed colocalization of both markers in the HSCs in the parenchyma (Fig. 4B–D).

Subsequently, to investigate the relationship between the distribution of LRAT+/CRBP-1+ cells and liver fibrosis, double immunofluorescence staining for LRAT and CRBP-1 was performed for all 24 cases. The number of LRAT+/CRBP-1+ cells/field was counted in 3 random fields each in the parenchyma, portal area and fibrous septa (only F3 and F4) in each case. The numbers in the upper left corner of each image indicate the average number of LRAT+/CRBP-1+ cells/mm^2. In the parenchyma, the number of LRAT+/CRBP-1+ cells in the space of Disse was not significantly different among F0-F4 (Fig. 5A–E). In the portal area, LRAT+/CRBP-1+ cells were hardly seen in normal liver (Fig. 5F). In F1 and F2, the LRAT+/CRBP-1+ cells were observed mainly at the periphery of the portal area (arrows) (Fig. 5G,H). The number of both positive cells was almost same in F1 and F2. In F3, F4, a large number of double positive cells were seen more than in F1 or F2 (Fig. 5I,J). In addition, in the fibrous septa in F3 and F4, a larger number of positive cells were seen than in the portal area of F3 or F4 (Fig. 5K,L).

Statistical analysis (Fig. 6) showed that the average number of positive cells in the parenchyma was not significantly different. The number of F0 in the portal area was statistically different from the number of F1 to F4 (a-b: $P < 0.005$; a-c: $P < 0.0002$; a-d: $P < 0.03$; a-e: $P < 0.04$). In addition, the average number of double positive cells was increased with the progression of fibrosis. Moreover, the average number of fibrous septa in F3 and F4 was statistically different from that of the portal area in F1 and F2 (b-f: $P < 0.005$; c-f: $P < 0.003$; b-g: $P < 0.0001$).

Discussion

HSCs in the space of Disse definitively contribute to fibrogenesis in parenchymal injury, such as alcoholic liver disease and non-alcoholic steatohepatitis, by transdifferentiation to activated HSCs (myofibroblasts). On the other hand, the origin of fibrogenic cells associated with portal fibrosis was unclear. Some agree that the

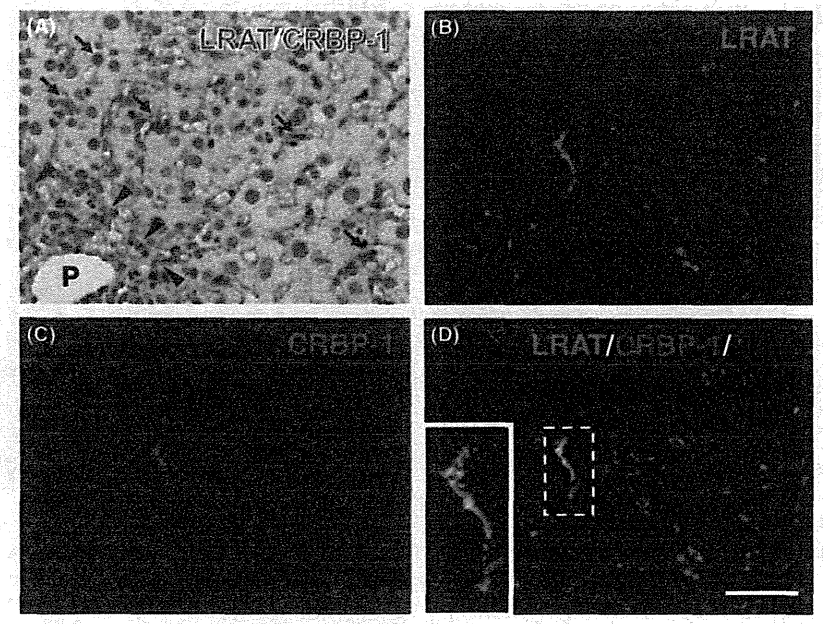

Fig. 4. (A) Double immunostaining for LRAT (red labelling) and CRBP-1 (brown labelling) of the human liver (METAVIR score of F2A2). LRAT+/CRBP-1+ cells were observed in HSCs in the parenchyma (arrows) and myofibroblasts in the portal area (arrowheads). (B–D) Double immunofluorescence staining for LRAT (green labelling) and CRBP-1 (red labelling) of human fibrotic liver with a METAVIR score of F2A2. The HSC in the space of Disse showed reactivity for LRAT (B) and CRBP-1 (C), and colocalization of LRAT and CRBP-1 (yellow double labelling) (D). Bar 20 μm.

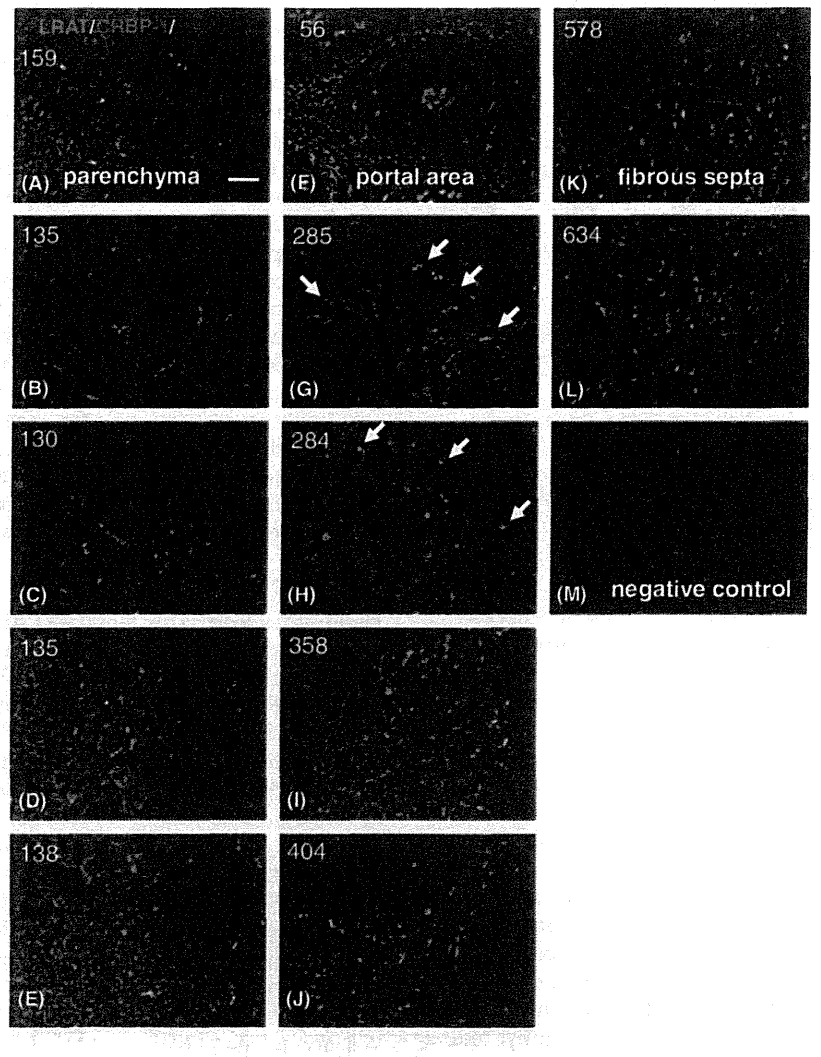

Fig. 5. Double immunofluorescence staining for LRAT and CRBP-1 in the parenchyma (A–E), portal area (F–J), and fibrous septa (K, L). The numbers in the upper left corner of each image indicate the average number of LRAT+/CRBP-1+ cells/mm^2. In the parenchyma, the number of LRAT+/CRBP-1+ cells in the space of Disse was not significantly different among the F0–F4 tissues (A–E). In the portal area, LRAT+/CRBP-1+ cells were hardly seen in the normal liver (F). In the F1 (G) and F2 (H) samples, LRAT+/CRBP-1+ cells were seen mainly at the periphery of the portal area (arrow). The number of both positive cells was almost the same in F1 and F2 tissues. In the F3 (I) and F4 (J) tissues, a large number of double positive cells were seen than in the F1 (G) or F2 (H) tissues. In addition, in the fibrous septa in F3 (K) and F4 (L) tissues, a larger number of positive cells were seen than in the portal area of F3 (I) or F4 (J) tissues. Negative control studies were also done using a Negative Control Rabbit IgG (M). Bar; 20 μm.

fibrogenic cells associated with portal fibrosis are portal fibroblasts (6, 40), or the cells derived from bone marrow (2–5); however, a few people believe that the fibrogenic cells are HSCs (41, 42). This study examined the *in situ* distribution of HSCs that expressed LRAT and CRBP-1 proteins was in human normal and pathological livers, particularly those with hepatitis B and C, to determine their contribution to HSCs on portal fibrosis. Some of the cells that coexpressed both LRAT and CRBP-1 were seen in the portal area and fibrous septa, especially in diseased liver. This result suggests that the cells that have the characteristic profile of HSCs can exist in the fibrous area. This suggests that HSCs in the space of Disse migrate from lobules to the fibrous area or are involved with the fibrous area, since these cells were particularly seen in fibrous expansion of the portal area and fibrous septa than in the portal tracts. These cells represented less than 20% of all cells/field (data not shown). Therefore, HSCs seem to partially contribute to a portal fibrosis. It is possible that cells other that HSCs mainly contributed to portal fibrosis. Ramadori *et al.* reported that the myofibroblasts in the fibrous septa closely resembled the (myo)fibroblasts in the portal field according to an immunohistochemical study using

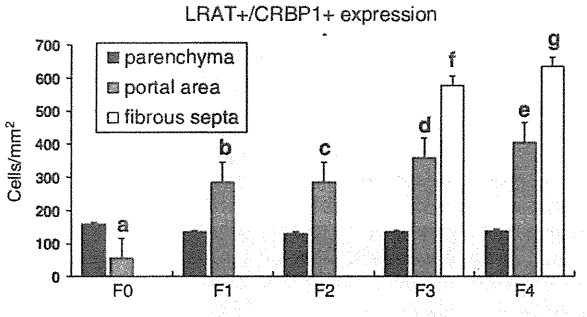

Fig. 6. The average ratio of the number of LRAT+/CRBP-1+ cells. The average number of positive cells in the parenchyma (black bars) was not significantly different. The number of F0 in the portal area (grey bars) was statistically different from the number of F1 to F4 (a-b: $P < 0.005$; a-c: $P < 0.0002$; a-d: $P < 0.03$; a-e: $P < 0.04$). In addition, the average number of double positive cells was increased with the progression of fibrosis. Moreover, the average number of fibrous septa (white bar) in F3 and F4 was statistically different from that of the portal area in F1 and F2 respectively (b–f: $P < 0.005$; c–f: $P < 0.003$; b–g: $P < 0.0001$).

in vivo HSC markers (6). Portal fibrogenesis may involve HSCs as well as portal fibroblasts.

We observed that the LRAT+/CRBP-1+ cells in the fibrous area did not contain lipid droplets in the cytoplasm, in contrast to the HSCs in the space of Disse. These cells apparently do not store vitamin A. Vitamin A from food absorbed from the small intestine is taken up by hepatocytes (liver parenchymal cells) in the form of retinyl ester through several metabolic steps (20). Retinyl ester is hydrolyzed to retinol again and bound to RBP4 in hepatocytes (43). A high concentration of retinol-bound RBP4 (holo-RBP4) in hepatocytes is secreted into the space of Disse. Excessive retinol likely diffuses into HSCs and becomes bound to CRBP-1. LRAT consists of esterified retinol to retinyl esters packed in lipid droplets in the cytoplasm. This vitamin A storing system is useful for maintaining the plasma retinol level at a nearly constant concentration (~1–3 × 10^{-6} mol/L) (43) to prevent toxicity because of hypervitaminosis A. The concentration of retinol in the space of Disse is apparently higher than that observed in the plasma following its release from hepatocytes after the ingestion of food. However, the concentration of retinol in the fibrous area seems to be similar to the plasma retinol level, since the blood supply in the fibrous area is from the portal veins or hepatic arteries. Since the retinol level as a substrate of LRAT is lower in the fibrous area than in the space of Disse, retinyl ester is not synthesized, even in LRAT+/CRBP-1+ cells. There are vitamin A storing-cells in other organs such as the lung, kidney, intestine and pancreas (7, 44–46). Definite lipid droplets in these sites are never seen under normal conditions, though lipid droplets increase in a rat hypervitaminosis A experimental model (44). In particular, pancreatic stellate cells are nearly identical to HSCs and both are presumed to share a common origin (47, 48). Stellate cells in other organs do not store vitamin A because of the lack of sufficient retinol as a substrate of LRAT as there is no microenvironment like the space of Disse which presents a high concentration of retinol . This condition is similar to the fibrous area in the human diseased liver under normal vitamin A conditions (normal nutritive status). Moreover, Fonseca *et al.* reported that fat-storing cells appear in the portal area and fibrous septa in chronic hepatitis model using C. hepatica-infected rats with hypervitaminosis A (42). This finding is consistent with the hypothesis that stellate cells in lobules migrate to the fibrous area including the portal area and contribute to fibrogenesis when liver damage occurs.

In conclusion, the present results provide direct evidence that the cells coexpressing both LRAT and CRBP-1 proteins contribute in part to the development of portal fibrogenesis in addition to parenchymal fibrogenesis in patients with viral hepatitis.

Acknowledgements

Financial support: This work was supported in part by grants, from the High Technology Research Center Project for Private University, from The Jikei University Research Fund, and from Grants-in-Aid for Scientific Research (#17590476, #19590572 and #22790673) by the Ministry of Education, Culture, Sports, Science and Technology in Japan, from the Program for Promotion of Fundamental Studies in Health Sciences of the National Institute of Biomedical Innovation (NIBIO), from JSPS Core-to-Core Program, A. Advanced Research Networks, and from the Research on the Innovative Development and the Practical Application of New Drugs for Hepatitis B (Principal investigator: Soichi Kojima; H24-B Drug Discovery-Hepatitis-General-003) provided by the Ministry of Health, Labor and Welfare of Japan (2012).

Conflicts of interest: The authors do not have any disclosures to report.

References

1. Bataller R, Brenner DA. Liver fibrosis. *J Clin Invest* 2005; **115**: 209–18.
2. Baba S, Fujii H, Hirose T, *et al.* Commitment of bone marrow cells to hepatic stellate cells in mouse. *J Hepatol* 2004; **40**: 255–60.
3. Kisseleva T, Uchinami H, Feirt N, *et al.* Bone marrow-derived fibrocytes participate in pathogenesis of liver fibrosis. *J Hepatol* 2006; **45**: 429–38.
4. Forbes SJ, Russo FP, Rey V, *et al.* A significant proportion of myofibroblasts are of bone marrow origin in human liver fibrosis. *Gastroenterology* 2004; 130: 1807–21.
5. Russo FP, Alison MR, Bigger BW, *et al.* The bone marrow functionally contributes to liver fibrosis. *Gastroenterology* 2006; **130**: 1807–21.
6. Ramadori G, Saile B. Portal tract fibrogenesis in the liver. *Lab Invest* 2004; **84**: 153–9.

7. Hinz B, Phan SH, Thannickal VJ, *et al.* The myofibroblast: one function multiple origins. *Am J Pathol* 2007; **170**: 1807–16. 38.
8. Sicklick JK, Choi SS, Bustamante M, *et al.* Evidence for epithelial-mesenchymal transitions in adult liver cells. *Am J Physiol Gastr Liver Physiol* 2006; **291**: G575–83.
9. Robertson H, Kirby JA, Yip WW, *et al.* Biliary epithelial-mesenchymal transition in posttransplantation reccurrence of primary biliary cirrhosis. *Hepatology* 2007; **45**: 977–81.
10. Zeisberg M, Yang C, Martino M, *et al.* Fibroblasts derive from hepatocytes in liver fibrosis via epithelial to mesenchymal transition. *J Biol Chem* 2007; **282**: 23337–47.
11. Ikegami T, Zhang Y, Matsuzaki Y. Liver fibrosis: possible involvement of EMT. *Cells Tissues Organs* 2007; **185**: 213–21.
12. Zeisberg EM, Tarnavski O, Zeisberg M, *et al.* Endothelial-to-mesenchymal transition contributes to cardiac fibrosis. *Nat Med* 2007; **13**: 952–61.
13. Iwaisako K, Brenner D, Kisseleva T. What's new in liver fibrosis? The origin of myofibroblasts in liver fibrosis *J Gastroen Hepatol* 2012; **27**: 65–8.
14. Yost RW, Harrison EH, Ross AC. Esterification of retinol bound to cellular retinol-binding protein. *J Biol Chem* 1988; **263**: 18693–701.
15. Matsuura T, Gad MZ, Harrison EH, Ross AC. Lecithin: retinol acyltransferase and retinyl ester hydrolase activities are differentially regulated by retinoids and have distinct distributions between hepatocyte and nonparenchymal cell fractions of rat liver. *J Nutr* 1997; **127**: 218–24.
16. Saari JC, Bredberg DL, Farrell DF. Retinol esterification in bovine retinal pigment epithelium: reversibility of lecithin: retinol acyltransferase. *Biochem J* 1993; **291**: 697–700.
17. Kurlandsky SB, Duell EA, Kang S, Voorhees JJ, Fisher GJ. Auto-regulation of retinoic acid biosynthesis through regulation of retinol esterification in human keratinocytes. *J Biol Chem* 1996; **271**: 15346–52.
18. Zolfaghari R, Ross AC. Lecithin: retinol acyltransferase expression is regulated by dietary vitamin A and exogenous retinoic acid in the lung of adult rats. *J Nutr* 2002; **132**: 1160–4.
19. Shingleton JL, Skinner MK, Ong DE. Retinol esterification in Sertoli cells by lecithin: retinol acyltransferase. *Biochemistry* 1989; **28**: 9647–53.
20. Ong DE, Lucas PC, Kakkad B, Quick TC. Ontogeny of two vitamin A-metabolizing enzymes and two retinol-binding proteins present in the small intestine of the rat. *J Lipid Res* 1991; **32**: 1521–7.
21. Randolph RK, Ross AC. Vitamin A status regulates hepatic lecithin: retinol acyltransferase activity in rats. *J Biol Chem* 1991; **266**: 16453–7.
22. Matsuura T, Ross AC. Regulation of hepatic lecithin: retinol acyltransferase activity by retinoic acid. *Arch Biochem Biophys* 1993; **301**: 221–7.
23. Shimada T, Ross AC, Muccio DD, Brouillette WJ, Shealy YF. Regulation of hepatic lecithin: retinol acyltransferase activity by retinoic acid receptor-selective retinoids. *Arch Biochem Biophys* 1997; **344**: 220–7.
24. Nagatsuma K, Hayashi Y, Hano H, *et al.* Lecithin: retinol acyltransferase protein is distributed in both hepatic stellate cells and endothelial cells of normal rodent and human liver. *Liver Int* 2009; **29**: 47–54.
25. Kato M, Blaner WS, Mertz JR, *et al.* Influence of retinoid nutritional status on cellular retinol- and cellular retinoic acid-binding protein concentrations in various rat tissues. *J Biol Chem* 1985; **260**: 4832–8.
26. Rajan N, Blaner WS, Soprano DR, Suhara A, Goodman DS. Cellular retinol-binding protein messenger RNA levels in normal and retinoid-deficient rats. *J Lipid Res* 1990; **31**: 821–9.
27. Blomhoff R, Rasmussen M, Nilsson A, *et al.* Hepatic retinol metabolism distribution of retinoids, enzymes, and binding proteins in isolated rat liver cells. *J Biol Chem* 1985; **260**: 13560–5.
28. Blomhoff R, Wake K. Perisinusoidal stellate cells of the liver: important roles in retinol metabolism and fibrosis. *FASEB J* 1991; **5**: 271–7.
29. Ong DE, MacDonald PN, Gubitosi AM. Esterification of retinol in rat liver: possible participation by cellular retinol-binding protein and cellular retinol-binding protein II. *J Biol Chem* 1988; **263**: 5789–96.
30. Herr FM, Ong DE. Differential interaction of lecithin-retinol acyltransferase with cellular retinol binding proteins. *Biochemistry* 1992; **31**: 6748–55.
31. Kato M, Kato K, Goodman DS. Immunocytochemical studies on the localization of plasma and of cellular retinol-binding proteins and of transthretin (prealbumin) in rat liver and kidney. *J Cell Biol* 1984; **98**: 1696–704.
32. Eriksson U, Das K, Busch C, *et al.* Cellular retinol-binding protein quantitation and distribution. *J Cell Biol* 1984; **259**: 13464–70.
33. Uchino K, Tuchweber B, Manabe N, *et al.* Celluler retinol-binding protein-1 expression and moduration during in vivo and in vitro myofibroblastic differentiation of rat hepatic stellate cells and portal fibroblasts. *Lab Invest* 2002; **82**: 619–28.
34. Lepreux S, Bioulac-Sage P, Gabbiani G, *et al.* Cellular retinol-binding protein-1 expression in normal and fibrotic/cirrhotic human liver: different patterns of expression in hepatic stellate cells and (myo) fibroblast subpopulations. *J Hepatol* 2004; **40**: 774–80.
35. Rossen EV, Borght SV, Grunsven LA, *et al.* Vinculin and cellular retinol-binding protein-1 are markers for quiescent and activated hepatic stellate cells in formalin-fixed paraffin embedded human liver. *Histochem Cell Biol* 2008; **131**: 313–25.
36. Bedossa P, Poynard T. An algorithm for the grading of activity in chronic hepatitis C The METAVIR Cooperative Study Group. *Hepatology* 1996; **24**: 289–93.
37. Schmitt-Graff A, Kruger S, Bochard F, Gabbiani G, Denk H. Modulation of alpha smooth muscle actin and desmin expression in perisinusoidal cells of normal and diseased human livers. *Am J Pathol* 1991; **138**: 1233–42.
38. Cassiman D, Libbrecht L, Desmet V, Denef C, Roskams T. Hepatic stellate cell/myofibroblast subpopulations in fibrotic human and rat livers. *J Hepatol* 2002; **36**: 200–9.
39. Cassiman D, Roskams T. Beauty is in the eye of the beholder: emerging concepts and pitfalls in hepatic stellate cell research. *J Hepatol* 2002; **37**: 527–35.
40. Beaussier M, Wendum D, Schiffer E, *et al.* Prominent contribution of portal mesenchymal cells to liver fibrosis in ischemic and obstructive cholestatic injuries. *Lab Invest* 2007; **87**: 292–303.

41. Marra F, Romanelli RG, Giannini C, *et al.* Monocyte chemotactic protein-1 as a chemoattractant for human hepatic stellate cells. *Hepatology* 1999; **29**: 140–8.
42. Fonseca YO, Lima CB, Santos ET, Andrade ZA. On the presence of hepatic stellate cells in portal spaces. *Mem Inst Oswaldo Cruz* 2005; **100**: 289–91.
43. Ross AC. Cellular metabolism and activation of retinoids: roles of cellular retinol-binding proteins. *FASEB J* 1993; **7**: 317–27.
44. Nagy NE, Holven KB, Roos N, *et al.* Storage of vitamin A in extrahepatic stellate cells in normal rats. *J Lipid Res* 1997; **38**: 645–58.
45. Wake K. 'Sternzellen' in the liver: perisinusoidal cells with special reference to storage of vitamin A. *Am J Anat* 1971; **132**: 429–62.
46. Omary MB, Lugea A, Lowe AW, Pandol SJ. The pancreatic stellate cell: a star on the rise in pancreatic diseases. *J Clin Invest* 2007; **117**: 50–9.
47. Buchholz M, Kestler HA, Holzmann K, *et al.* Transcriptome analysis of human hepatic and pancreatic stellate cells: organ-specific variations of a common transcriptional phenotype. *J Mol Med* 2005; **83**: 795–805.
48. Erkan M, Weis N, Pan Z, *et al.* Organ-, inflammation- and cancer specific transcriptional fingerprints of pancreatic and hepatic stellate cells. *Mol Cancer* 2010; **9**:88.

Anal Bioanal Chem (2013) 405:8073–8081
DOI 10.1007/s00216-013-7056-1

RESEARCH PAPER

Examination of an absolute quantity of less than a hundred nanograms of proteins by amino acid analysis

Akiko Masuda · Naoshi Dohmae

Received: 30 January 2013 / Revised: 14 March 2013 / Accepted: 8 May 2013 / Published online: 30 May 2013

Abstract We developed an ultra-sensitive method of amino acid analysis (AAA) for the absolute quantification of less than 100 ng of proteins, in solution or on polyvinylidene difluoride (PVDF) membranes using an oxygen-free chamber for protein hydrolysis. We used a pre-label method with 6-aminoquinolyl-*N*-hydroxysuccinimidyl carbamate for fluorescence detection, ion-pair chromatography with a reversed-phase column, and an ultra-high-pressure high-performance liquid chromatography. We optimized both handling- and instrument-dependent factors for accurate quantification and showed that the least amount of proteins to quantify was determined by handling accuracy rather than instrumental limit for quantification which was 0.6 fmol/amino acid. As a new evaluation method for the handling accuracy, we adopted the protein identification by the obtained amino acid compositions by AAA and the Swiss-Prot database search without the restriction of species. As a result, the least amount of starting material for AAA was 16 ng (0.24 pmol) for a solution of bovine serum albumin (BSA), 33 ng (0.50 pmol) for BSA on a PVDF membrane, and 44 ng (0.15 pmol) for thyroglobulin on a PVDF membrane. These results demonstrate that the ultra-sensitive AAA developed in this study is feasible for absolute quantification of biological significant protein.

Keywords Amino acid analysis · Protein quantification · Post-translational modifications · Absolute quantification · Protein hydrolysis · Proteomics

Published in the topical collection *Amino Acid Analysis* with guest editor Toshimasa Toyo'oka.

A. Masuda · N. Dohmae (✉)
Biomolecular Characterization Team, RIKEN,
2-1 Hirosawa, Wako,
Saitama 351-0198, Japan
e-mail: dohmae@riken.jp

A. Masuda
e-mail: aki@riken.jp

Introduction

Amino acid analysis (AAA) is classic but plays an important role as quantitative method in many biological, biomedical, and food analyses. AAA has been used for determination of absolute amount of free amino acids, peptides, or proteins not just for amino acid composition of proteins. The quantitative accuracy of AAA has recently been noted again and many applications have been reported [1–6]. In proteomics, mass spectrometry (MS) has become the most informative tool and has replaced AAA as a qualitative technique and also, most recently, as a quantitative method. Quantitative MS requires an accurate amount of peptide or protein calibrants; but gravimetric method based on the weighing of solid analyte is unsuitable for the purpose since peptides or proteins often contain unknown amount of bound salts and/or hydrated water. AAA has become an important quantitative method in obtaining absolute amount of these calibrants. Another benefit is that AAA is free of bias by the amino acid sequence of proteins since the proteins are completely hydrolyzed to the constituted amino acids before AAA. Therefore, AAA is applicable to the proteins that are not easy to be analyzed by sequence-dependent enzymatic proteolysis plus MS such as Lys- and Arg-rich histones (histones are inappropriate for application of MS with enzymatic proteolysis, because histones have many modifications on Lys and Arg residues that prevent a usage of typical enzyme such as trypsin cleaving the carboxyl side of Lys or Arg) or membrane proteins that possess large hydrophobic moiety. A previously unknown histone modification, hydroxylation of Lys, was recently identified and quantified by AAA [2]. In another example, the 3D structure of a membrane protein in solution predicted by molecular dynamics simulations was experimentally confirmed from quantification of intramolecular Cys–Cys bond formation by AAA [3] (distance between two Cys residues of the membrane protein can be estimated by quantification of

intramolecular Cys–Cys disulfide bond formation since the disulfide bond is formed when the two residues are positioned enough close to each other).

In the early 1950s, AAA was originally accomplished by separation of amino acids with ion-exchange chromatography, labeling of the amino acids with ninhydrin, and detection of them by visible light absorbance [7, 8]. The sensitivity of the AAA with the ninhydrin detection is not sufficient for small amount of proteins. Therefore, many sensitive methods for detection of amino acids have been developed based on chemical modifications of amino acids for fluorometry [9–12] or MS [13–15] before amino acid separation by liquid chromatography (LC), i.e., pre-column derivatization. In the pre-column derivatization, the hydrophobicity of amino acids can be enhanced, facilitating their separation by reversed-phase chromatography, which prevents dilution of peaks and enhances the sensitivity of detection. These pre-column labeling methods provide femtomole to picomole sensitivity to AAA [16, 17]. In this study, we quantified amino acids by a pre-column derivatization with 6-aminoquinolyl-*N*-hydroxysuccinimidyl carbamate (AQC) for fluorescence detection because of three reasons: the reagent react with all amino acids including the secondary amino acids, the derivatized amino acid are stable at room temperature, the derivatization reaction is linear with amount of amino acids, and the excess reagent does not disturb analysis [12].

Because of development of highly sensitive AAA, quantification of free amino acids can be readily achieved in sub-picomole level, but obtaining accurate quantity of low-abundance proteins (less than 100 ng) after hydrolysis steps without or less contamination from environment is far more difficult [18, 19]. For accurate quantification of amino acids in protein samples, following three requirements must be satisfied.

First, protein samples must be purified and rendered homogeneous before hydrolysis, because the amino acids of contaminant proteins cannot be distinguished from those of the sample proteins. A favorite method for preparation of homogeneous protein samples is sodium dodecyl sulfate-polyacrylamide gel electrophoresis (SDS-PAGE) because of its inherent high resolution and simplicity. Direct hydrolysis of proteins in polyacrylamide gels causes the liberation of large quantities of ammonia, which hinders the use of AAA because the excessive ammonia consumes the reagent used for the pre-column labeling of amino acids. To circumvent this issue, the separated proteins are electroblotted onto a polyvinylidene difluoride (PVDF) membrane and hydrolyzed on the membrane [20, 21]. If the protein to quantify is not isolated from other proteins, the amount of the protein is unknown, whereas the total amount of protein mixture can be known by sum of multiplying amino acid amount by the each residual mass. Second, protein samples should be completely and quantitatively hydrolyzed to amino acids.

Many hydrolysis methods that utilize enzymes, strong bases, or strong acids are available, and the proper method depends on the aim of the analysis [22]. Hydrolysis using hydrochloric acid (HCl) is currently universally applied to AAA, because HCl can cleave peptide bonds completely independent of the amino acid sequence and can easily be removed from hydrolysates by evaporation. Except for labile or inert amino acids under acidic conditions, most amino acids are obtained quantitatively from proteins by hydrolysis with HCl (see details in the "Experimental section"). Furthermore, we have developed an automated hydrolysis system using a solid acid catalyst, which yielded over 70 % of the amino acids recovered after conventional hydrolysis of proteins with HCl [23]. Since the automated system cannot be used for hydrolyzing electroblotted samples, HCl was used in this study.

Third, contamination from environment during many complicated operations, SDS-PAGE, electroblotting, and hydrolysis, must be prevented or restricted. Among them, the hydrolysis of proteins is responsible for most analysis errors and a precise technique for handling small amounts of samples is necessary. Then a sufficient amount of protein, typically from one to several micrograms, has been used to overcome the contribution from potential contaminants for obtaining an accurate amino acid composition [17, 18]. In the previous work, highly sensitive AAA was reviewed, in which 0.5 μg of bovine serum albumin (BSA) in solution was hydrolyzed and a part of them, 45 and 100 ng, was quantified [16]. Cohen et al. investigated in detail the relationship between hydrolyzed protein amount of sample solution and average errors in the composition dividing the categories according to the protein amount: trace analysis (<100 ng), high sensitivity (100–500 ng), low intermediate (500–100 ng), high intermediate (1,000–2,000 ng), and high (>2,000 ng) [18]. They also showed similar investigation of dot-blotted protein solution to membranes collected from capillary electrophoresis [24]. In both cases, a steady increase in the average error as sample amount decreases was observed. At the high sensitivity range for proteins on the membrane and at the trace analysis range for protein solutions, the average errors in the composition reached around 20 % [18, 24]. The reduction of the contamination from environment is most critical for accurate quantification of low-abundant proteins. The purpose of this study is that the method to obtain meaningful results from trace analysis (the amount hydrolyzed<100 ng of proteins both in solution and on membrane) is established by improving both handling- and equipment-dependent factors. The accuracy of AAA for less than 100 ng of proteins was evaluated by the accuracy of amino acid composition and by assessing whether analyzed proteins were correctly identified from the obtained composition using the Swiss-Prot database. Only ten or a few tens of nanograms of BSA in solution or on a blotted membrane and thyroglobulin (TG) on a blotted membrane were correctly